I.O.S.

A PROGRESS REPORT ON THE NARROW BEAM ECHO – SOUNDER

by
M.L. SOMERS

REPORT NO. 12
1975

NATURAL ENVIRONMENT RESEARCH COUNCIL
INSTITUTE OF OCEANOGRAPHIC SCIENCES

INSTITUTE OF OCEANOGRAPHIC SCIENCES

A PROGRESS REPORT ON THE NARROW BEAM ECHO-SOUNDER

by

M. L. SOMERS

with contributions by

DR. H. O. BERKTAY

(Dept. of Electronic Engineering, University of Birmingham)

REPORT NO. 12

1975

Institute of Oceanographic Sciences,
Wormley, Godalming,
Surrey, GU8 5UB.

CONTENTS

The Narrow Beam Echo-Sounder - A Progress Report

Introduction

The precision echo-sounder has become a key tool in marine science. Immediately following its introduction in the late 1950's so little was known of deep sea bathymetry that the data rate from the new machines was enormous, and there was a tendency to overlook its short-comings, in particular the acoustic beam pattern, and the errors that a wide beam can introduce. In what follows we go briefly through the acoustic design considerations for an echo-sounder system and the effects of the acoustic beam pattern. Then we look at the conventional means of obtaining a narrow acoustic beam. This is followed by a look at the concept of non-linear generation of narrow beams with a summary of the theory. Then we consider the project jointly undertaken by IOS and the University of Birmingham, with some results from the preliminary trials. The report ends with a summary of the necessary work remaining, before the narrow beam echo-sounder is a working reality.

Echo-Sounding in General

The echo-sounder has been described too often in concept and operation to need repetition here, nor will we deal with depth errors due to velocity variation or other causes, but we begin with a consideration of the acoustic performance.

Equation 1 is an expression for the intensity of the acoustic pulse reaching the bottom at an angle θ to the vertical below the transducer, assuming the axis at the latter is vertical.

$$I_\theta = \frac{p^2}{\rho c} = \frac{1}{4\pi} \frac{P}{D^2} R(\theta) \; e^{-\alpha D} \qquad (1)$$

Where P is the acoustic pressure, ρ is the density, c the velocity of sound, P the total radiated power and D the depth. $R(\theta)$ is the directivity factor, which is a measure of the concentration of power along the transducer axis. It depends on the width of the transducer face in terms of the wavelength of sound. The quantity α is the attenuation factor which increases as the square of the frequency. The dilemma faced by the designer is that with a transducer of reasonable physical size, a narrow beam which requires a high directivity factor, can only be obtained by using a high frequency, and this incurs a high penalty in terms of attenuation, which cannot be offset by increasing the transmitter power P, due to cavitation at the transducer face.

If there is a small object in the path of the beam it will intercept a power $I_\theta \times S$, where S is the cross-sectional area presented to the beam by the object. A proportion of this intercepted energy is re-radiated or scattered in various directions depending on the size and orientation of the target. The proportion of incident energy re-radiated depends upon the acoustic transparency of the target and its damping. To maintain formal simplicity in the treatment of reflection a fictional cross-section area τ is assigned to the target such that the echo from the actual target is the same as that from a perfect reflector of cross-section area σ. To take account of the directional properties of the target σ is made a function of angle thus $\sigma(\theta)$. Generally σ is smaller than the geometrical cross-section, but it is not invariably so, for example the acoustic cross-section of a bubble at resonance greatly exceeds its physical cross-section.

The acoustic intensity reflected from the target at the transducer is given by:-

$$I_T = I_\theta \frac{\sigma(\theta)}{4\pi} \cdot \frac{1}{D^2} e^{-\alpha D} \qquad (2)$$

$$\text{or } I_T = \frac{P}{4\pi} \cdot R(\theta) \frac{\sigma(\theta)}{4\pi} \frac{e^{-\alpha D}}{D^4} \qquad (3)$$

and it is the ratio of this intensity to the noise power in the receiver bandwidth which determines the detectability of the target. If the target occupies an appreciable portion of the beam, and the bottom invariably occupies it all, equation 3 has to be integrated over the limits of the target paying due regard to the phases of the reflections.

In the case of a perfectly flat bottom, which need not be either level or perfectly reflecting, the result of integrating equation 3 is particularly simple, for the bottom is a plane lossy mirror and the reflected intensity is given by equation 4

$$I_T = \frac{P}{4\pi} R(\theta) \frac{e^{-2\alpha D}}{4D^2} \beta \qquad (4)$$

where β is the proportion of energy reflected by the bottom.

The usual case of a rough bottom is more complicated. In principle equation 3 can be integrated for any transmitter/receiver position, but it would have to be done for each such position, and the bottom topography and reflectivity would have to be known. In practice an acoustic model of the bottom is constructed based on its statistical properties, and estimate of bottom echoes are made. This is the subject of the next section. The fore-going is treated in greater detail in Camp /1/ Chap.9.

Back Scattering from the Sea Floor

The following treatment of the problem is adapted from Tolstoy and Clay /2/ Chap.6. Sound reflected from a plane mirror surface has the same properties as the incident sound, and none is scattered in any direction but the specular one. The scattering is coherent since there are definite phase relationships between the incident and scattered wave. Translation of the surface in its plane does not have any effect on the reflection. Such a surface is of course a fiction, which is only closely approached at echo-sounding frequencies in the abyssal plain areas of the oceans. One approach to modelling the bottom is to regard it as made up of a large number of specular reflectors of random size and slope, each with its own diffraction pattern. By making the reasonable assumption of a Rayliegh distribution of reflector size and Gaussian distribution of slope and treating each reflector as a line reflector it is possible, as Patterson /3/ did to arrive at an expression for back-scattering as a function of angle which fits the observed form of the curve. However lack of frequency dependence of this curve only comes out of the model with some rather artificial assumptions.

A more satisfactory approach is to try to evaluate the scattered acoustical pressure by means of the Helmholtz theorem. Tolstoy and Clay do this under the assumption of a directional source and the Kirchhoff approximation which is that the wave is locally reflected by a plane surface. The Kirchhoff approximation is valid in regions where there is no shadowing and the radius of curvature is much greater than the acoustic wavelength.

The scattered acoustical pressure is given by

$$p(D') = \frac{1}{4\pi}\int_s \left(p\Big|_s \frac{\delta\psi}{\delta n} - U \frac{\delta p}{\delta n}\Big|_s \right) dS \qquad (5)$$

where $\Psi = \dfrac{e^{j(kD' - \omega t)}}{D'}$, S is the illuminated area of the bottom, n is the normal to S directed toward the source. $p\Big|_s$ and $\dfrac{\delta p}{\delta n}\Big|_s$ are the values of p and its normal derivative on the surface S. The origin of coordinates is the centre of illuminated area and the mean bottom surface is the xy plane. The source and receiver are assumed to be far removed from the area S, and the latter is much larger than the wavelength.

Tolstoy and Clay simplify the Helmholtz Integral (5) by using a gaussian illumination function of small angular extent, and averaging the reflection coefficient over the illuminated area. The reflection coefficient R at any point under the Kirchhoff approximation is given by:-

$$R = \frac{p'c'\cos\theta - pc\cos\theta'}{p'c'\cos\theta + pc\cos\theta'} \qquad (6)$$

where θ is the angle of incidence p', c' refer to the seabed material and θ and θ' are connected by Snells law. Their expression for the scattered pressure, p, in the situation depicted in Fig. 1 is

$$p = jkP_0 \frac{\rho c}{2\pi} f(\theta) \frac{Re^{jk(r_1 + r_2)}}{2\pi r_1 r_2} \int_{-\infty}^{\infty}\int D_0 \, e^{2j(\alpha x + \beta y + \gamma\zeta)} \, dy \, dx \qquad (7)$$

where

$$f(\theta) = \frac{1 + \cos\theta_1 \cos\theta_2 - \sin\theta_1 \sin\theta_2 \cos\theta_3}{\cos\theta_1 + \cos\theta_2} \qquad (8)$$

and α, β, γ are the wave number differences between the incident and scattered wave in the x, y and z directions, and ζ is the elevation of the surface from the mean in the z direction. D_0 is the illumination function.

$$D_0 = e^{-\frac{x^2}{2x^2} - \frac{y^2}{2y^2}} \qquad \text{for gaussian illumination.}$$

Under the approximations used equation 7 applies to any surface, and Tolstoy and Clay apply it first to a periodic surface for which the results can be verified by experiment. Then by considering the statistics of the signal fluctuations in relation to those of the surface for a gaussian surface they arrive at a scattering function. The surface displacement ζ is given by the probability function

$$W(\zeta) = \frac{1}{\sigma\sqrt{2\pi}} e^{-\frac{\zeta^2}{2r^2}} \qquad (9)$$

The difference between the incident and reflected wave numbers have horizontal and vertical components:-

$$\alpha = \frac{k}{2} (\sin \theta_1 - \sin \theta_2 \cos \theta_3)$$

$$\beta = -\frac{k}{2} \sin \theta_2 \sin \theta_3$$

$$r = -\frac{k}{2} (\cos \theta_1 + \cos \theta_2)$$

For the case of backscattering $\theta_3 = 0$ and $\theta_2 = \theta_1$. hence $\alpha = k \sin \theta$. $\beta = 0$, $\gamma = -k \cos \theta$.

Tolstoy and Clay distinguish two regimes where the parameter $\gamma\sigma$ is respectively much less than unity, the low frequency case, and much greater than unity, the high frequency case, which approaches the low frequency case for θ approaching $\pi/2$ or grazing incidence. In the latter case shadowing is important enough to invalidate the theory.

For the low frequency (small $\nu\tau$) case they find incoherent scattering function

$$S_{1f} = \frac{2}{\pi} R^2 \nu^2 \sigma^2 f^2(\theta) \, k^2 (r_0')^2 \, e^{-4r^2\tau^2 - 2(Kr_0')^2} \qquad (10)$$

where R is given by equation (6), $f(\theta)$ by equation (8) and r_0' is related to the horizontal scale of the surface roughness and the illuminated area by

$$\frac{1}{(r_0')^2} = \frac{1}{r_0^2} + \frac{1}{(R')^2} \qquad (11)$$

in which R is the effective radius of illumination and r^0 is given by the isotropic gaussian correlation function:-

$$\psi = e^{-\frac{r^2}{2r_0^2}}$$

K is a new variable introduced for the purpose of evaluating an integral, and has the value $\alpha / \cos \theta$.

For back-scattering we have $K = k \tan \theta$ since $\alpha = k \sin \theta$ and $f(\theta) = 1/\cos \theta$.

Thus in the low frequency case the angular dependence resides only in the exponential term, since the dependence in γ^2 cancels that in $f^2(\theta)$. The effective exponential term is

$$e^{-4k^2\sigma^2 \left(1 + \frac{(r_0')^2}{2\sigma^2} \frac{\tan^2 \theta}{\cos^2 \theta} \right)}$$

This result shows a very rapid and peaking variation of back-scattering with frequency in the region where $(2\nu\tau) < 1$ or $\sigma < n/4\pi$ and thus only applies to a very smooth surface. The frequency dependence increases with angle towards grazing incidence depending upon the effective bottom slopes which are measured roughly by σ/r_0'. At normal incidence the coherently reflected component is of greatest importance.

For the high-frequency (large $\nu\tau$) case Tolstoy and Clay give an expression:-

$$S_{hf} = \frac{R^2}{8\pi \cos^4 \theta \, \langle \zeta'^2 \rangle} \, e^{-\frac{K^2}{2\nu^2 \langle \zeta'^2 \rangle}} \qquad (12)$$

where $\langle \zeta'^2 \rangle$ is the mean square surface slope near the centre of the illuminated patch. The frequency dependence has dropped out of this expression as can be seen by substituting for K and γ when we get

$$S_{hf} = \frac{R'^2}{8\pi \cos^4\theta \langle \zeta'^2 \rangle} e^{-\frac{2 \tan^2 \theta}{\langle \zeta'^2 \rangle \cos^2 \theta}} \qquad (13)$$

The coherent reflected energy is negligible at all angles of incidence.

The actual received signal takes the form

$$\langle s^2 \rangle = \frac{P_0 \rho c}{8D^2} S_{hf} \qquad (14)$$

where $\langle s^2 \rangle$ is the expected value of the mean squared pressure at the receiver, D is the depth. This holds provided the transmitter directivity is fairly high (for example $\geq$ 20 dB) and the angle of incidence is not too great, for then the pulse length limits the area of bottom illuminated at any time, and shadowing effects start to appear.

SHF has the general form shown in the figure for $\langle \zeta'^2 \rangle$ 20×10^{-3}/ 5×10^{-2} r.m.s. slopes of about 10^o and 5^o for a value of R' near unity.

We see a strong dependence on θ and a fairly strong dependence on r.m.s. slope. At 10 kHz the smoother sea bottoms such as sand or mud fall between the low and high frequency cases, and one would expect an even more rapid fall off of backscattering, but these results give a qualitative explanation of some observations made on the first trials of the narrow beam sounder.

The Effects of a Finite Transducer Beam Pattern

In the foregoing treatment of back-scattering the acoustic beam pattern was assumed to be both narrow and of Gaussian shape. That is to say the intensity in a direction θ to the acoustic axis was given by:-

$$I(\theta) = \frac{I_0}{\sigma\sqrt{2\pi}} e^{-\frac{\theta^2}{2\sigma^2}} \qquad (15)$$

The practical implications of trying to achieve a Gaussian beam pattern are discussed in the next section. Actual transducers in use are usually square arrays with sides about 3 wave-lengths long consisting of 9, 16 or 25 elements depending upon the type of transducer in use. In any case very little error occurs if the transducer is considered as a uniformly illuminated square aperture. It is also usual to assume that the transducer operates in a perfect baffle, and again the practical errors resulting from this assumption are fairly small at least out to the first side-lobe. The beam pattern of such a transducer is easily deduced to be

$$p(\theta) = p_0 \frac{\sin\left(\frac{kl}{2} \sin\theta\right)}{\frac{kl}{2} \sin\theta} \qquad (16)$$

in either principal plane. Off the principal planes the pattern is that of a line source with a strength distribution equivalent to the sum of strengths along a line perpendicular to it at that point. Camp /1/ Chapter 7 gives a typical treatment, and fig.3 shows the beam pattern in a principal plane of a transducer 3 wavelengths wide. It can be seen that appreciable energy is emitted at angles up to 60 degrees from the axis, the second side lobe being only 18 decibels below the main beam. If this information is considered in conjunction

with figure 2 it will be appreciated that considerable errors can frequently occur when the first returning echo is taken as the depth vertically below the transducer. For instance over a uniform bottom slope of 10^{o} there is an error of 1.5% in the indicated depth. Also a feature some distance off the transducer axis can show up quite strongly. This is particularly evident on echo-sounding records over very rough terrain where each bottom feature has a long hyperbolic 'signature', as in Fig. 4. It is quite easy to set up hypothetical situations in which various misleading artefacts appear on the record.

From this discussion it can be seen that the shortcomings of wide-beam echo-sounders can arise from either the width of the main lobe or the presence of sidelobes, and in the development of a narrow beam echo-sounding system both effects have to be considered.

Conventional Narrow Beam Transducers

It is obvious that any transducer has to be stabilised to within its own beam width for the duration of the pulse repetition period, and a narrow beam transducer must be stabilised to within its own beamwidth of the vertical to avoid throwing away the greater precision resulting from the reduced beamwidth. Thus there arises at once the question of whether the array is to be passively stable within a fairly narrow angular range, or gyroscopically stabilised within a very narrow angular range. Equation 15 indicates that the beamwidth between the half-power points of the main lobe is inversely proportional to the linear dimension of the array at any frequency; so in order to avoid the problems and expense of stabilising a very large array it is important to put up with the widest possible beam angle, provided it is significantly narrower than the 20^{o} of the first generation ech-sounder. If we take a specific case the problems can be illustrated. Assume that we wish to obtain a 3^{o} beam between half power points and that we decide the largest practical diameter for stabilisation purposes (to within the beam) is 1 metre. The pattern of a circular array is given by $P(\theta) = P_o \, 2 J_1(x)/x$

where $x = \frac{2\pi a}{\lambda} \sin\theta$ and $J_1(x)$ is the first order Bessel function.

This has half power points where $x = 1.615$ whence $\lambda = 4.9$ cms for $\theta = 1.5^{o}$ and $f = 30$ KHz is the required operating frequency. The approximate calculation of signal to noise ratio over a flat bottom at 5 Km depth proceeds as follows:-

Power density at 30 KHz is about 0.5 Watts/cm^2, so $P_o = 3.9$ KW. This is + 36dB re 1 watt.

This has to be enhanced by the transmitting directivity of the array which is approximately $20 \log_{10} \frac{360}{\theta}$, where θ is the full half power beamwidth, or 41.6dB. So the total source level re 1 mBar at 1 metre is

$$p_o = 71.6 + 36 + 41.6 = 149.2\text{dB}$$

The losses are	spreading loss $- 20 \log_{10} R$	= 80dB
	attenuation at 9.2dB/10^3m	= 92dB
	Bottom loss	= 12dB
		= 184dB

hence the free field level of bottom echo at the transducer is - 34.8dB re 1 mBar. The free field noise spectrum level is very roughly - 15dB re 1 mBar 1 in 1 Hz band, which has to be reduced by the directivity to get - 56.6dB and then increased by the detection bandwidth which we may take as 500 Hz for a

2 mS pulse length (this gives 1 fathom resolution). The bandwidth correction is 27dB. So the final signal to noise ratio = - 34.8 + 56.6 - 27dB or - 5.2dB.

To improve this signal to noise ratio we can increase the source level which can only be done by increasing the size of the array. If we attempt to do so by increasing the operating frequency the attenuation losses increase much faster than the source level. A 2 metre array would give a 12dB better signal level - 6dB from directivity and 6dB from greater radiating area at the same power density, but we would have stepped outside our mechanical limits, by requiring better stabilisation for a larger array. The signal/noise ratio can also be improved by reducing the losses which means reducing the frequency, and accepting a wider beam, but the loss of angular resolution can be quite small. For instance in the case above a reduction of frequency by 10% results in a total signal/noise improvement of about 15dB taking the various directivity factors, power levels and noise levels into account, and this is achieved with a 3.3^{o} beam. The designer would probably find this an irresistably attractive compromise.

The sidelobes of the 1 metre diameter array at 27 KHz fall off fairly rapidly but there is one only 32dB below the axial level at 15^{o} from the axis, so that although the objectionable effects of sidelobes have been very much reduced they have not been eliminated, and it is easy to see that the practical problems of doing so are severe. Camp /1/ gives an outline of the Dolph-Tschebyscheff method of shading a linear array to achieve a given side lobe level for a minimum increase in the main beam, and maximum power level. The power level must fall when shading an acoustic array since the peak power density is fixed so shading can only be achieved by a reduction in nett power density. The Dolph-Tschebyscheff procedure applied to a 10 wavelength square array, shaded in both directions with 10 sections in each direction (i.e. 100 array sections) gives for a side-lobe level of -40dB an increase in main lobe width from 3.0 degrees to 3.6 degrees but at a loss of power amounting to 7.3dB or 80%. At the lower frequency the main beam angle would be about 4^{o}, with similar shading, and the signal/noise ratio over a flat bottom at 5 Km would be about +3dB. These figures assume a rather high ship noise, so the design is quite feasible and the stabilisation could be achieved. In fact the German research vessel R/V Meteor is fitted with a 1 metre square array, but without, as far as is known, any shading.

A New Approach to Narrow Beam Formation

Classical acoustics is based on an approximation, which is used in deriving a linear wave equation. The approximation is that acoustic pressures are so small that they have no effect on the compressibility of the fluid. At high acoustic intensities departures from linearity, though small, are no longer negligible, and two acoustic fields in the same region will not superpose linearly. This leads to the concept of one acoustic wave being scattered by a second, and in a paper in 1957 Westervelt /4/ examined the conditions under which the scattered wave was appreciable and derived an expression for its magnitude in terms of the field distribution of the primary acoustic waves. Since then the subject has engaged the attention of a number of workers including Dr. Berktay of Birmingham University to whom the following simplified account of the theory is due.

Briefly, in a parametric transmitter two waves of relatively high frequency are transmitted simultaneously from a single transducer assembly. The nonlinear interaction of these two primary waves results in the production of a low frequency wave (at the difference-frequency of the primary waves) as well as other interaction-frequency components. The phasing of the difference-frequency component produced at various parts of the interaction volume is such that these wavelets add co-phasally in the "end-fire" direction, i.e., along the axis of the superposed primary beams. As a consequence of these virtual sources in an end-fired array configuration, narrow beams can be obtained at relatively low frequencies.

Parametric Transmitting Device

General

The characteristics of parametric transmitters are discussed in some detail in the Appendix. Only a summary of the results will be presented in this section. The considerations are limited to the case where a square transducer is used to launch the primary waves. The results for circular transducers are very similar, while those for rectangular transducers may be found in the literature (see reference 6).

In a parametric transmitting device, the beamwidth at the difference-frequency is controlled by two parameters:-

(a) Absorption of the primary waves introduces an exponential taper on the end-fired array,

(b) The beamwidth of the primary waves controls the shape of the interaction volume, and of the end-fired array.

The effects of absorption alone would result in a difference-frequency beam of width (see Equations 12-17 in the Appendix) $2\theta_d$, where

$$\theta_d = \sqrt{2\alpha_T / k_-}$$

k_- is the wave-number at the difference-frequency, and α_T is an absorption parameter given by

$$\alpha_T = \alpha_1 + \alpha_2 - \alpha_-$$

Here the subscripts 1 and 2 indicate the values of the absorption coefficient at the two primary frequencies, and (-) that at the difference-frequency. Normally, $\alpha_- \ll \alpha_{1,2}$ hence α_T is very largely controlled by the mean primary frequency, while k_- represents the dependence of θ_d on the difference frequency.

If the primary-waves are transmitted from a square transducer of sides ℓ, the 3dB beamwidth (calculated for a mean primary frequency ω_0) would be given by

$$2\gamma_1 = (2\sqrt{2}/\pi)\ (\lambda_0/\ell)$$

As shown in the Appendix, the ratio of the 3dB beamwidth at the difference-frequency to $2\theta_d$ is a unique function of the parameter

$$\psi_y = \gamma_1 / \theta_d$$

This relationship is shown (the solid curve) in Fig.13. Also shown in Fig.13 (the dashed curve) is the dependence of the ratio of the beamwidth at the difference-frequency to the primary beamwidth (i.e., $2\gamma_1$) on ψ_y. This latter curve shows that for $\psi_y \geq 1$, the difference-frequency waves are confined to a beam the width of which is of the order of $2\gamma_1$, and the influence of ψ_y is very small. In other words, for this range of values ψ_y, the beamwidth at the lower frequency is largely controlled by that of the primary waves. [This geometric, rather than diffraction, control of the beam pattern provides the possibility of producing constant beamwidth over a wide range of values of the difference-frequency.]

In a sonar application of a transmitting device, the other parameter of interest is its effective source level.

It is shown in the Appendix that the effective source level (at the difference-frequency) of a parametric transmitter is given by

$$(SL_-) \simeq -186.7 + 20 \log F_- + (SL)_1 + (SL)_2 + 20 \log \frac{|V|}{\alpha_T r_0} \quad \text{dB rel } \mu\text{bm},$$

where $(SL)_1$ and $(SL)_2$ are the primary source levels (all source levels are for r.m.s. values, and in dB rel μbm), F_- is the difference-frequency in kHz, and $|V| / \alpha_T r_0$ is related (uniquely, for a square transducer) to ψ_y. Dependence of $20 \log [\, |V| / \alpha_T r_0 \,]$ to ψ_y is shown in Fig.14.

The foregoing results are applicable provided the transmitted acoustic intensities are such that the primary waves do not form shock within the nearfield of the transducer. This condition may be represented as an upper limit on the primary source levels (see Equation 43 in the Appendix) in the form

$$(SL)_{1,2} \leq 137 + 20 \log \lambda_0 \text{ cm} \quad \text{dB rel } \mu\text{bm}$$

or

$$(SL)_{1,2} + 20 \log F_0 \leq 180.5, \quad \text{dB rel } \mu\text{bm}$$

where F_0 is the primary frequency in kHz.

If the primary source levels exceed this value, the extent to which variations may be expected from the results discussed above depends on the value of the acoustic Reynolds number.

If the primary source levels exceed this limiting value significantly, then the difference-frequency beam would be expected to be wider, and the effective source level lower, than the estimates made on the basis indicated above. Therefore, for a narrow-beam echo-sounder, it would be wise to avoid these high intensity effects by a suitable choice of the design parameters.

Design Considerations

With the difference-frequency and the beamwidth fixed, the parameters to be selected are the primary frequency and the transducer size. However, it must be pointed out that there is not a unique design to satisfy these requirements. It is possible, though cumbersome, to go through a process of optimization. However, some basic arguments simplify this process considerably.

The required beamwidth can be obtained either by making $\psi_y < 1$ (which results in the beamwidth being approximately equal to $2\theta_d$), or by choosing $\psi_y \geq 1$.

If $\psi_y < 1$, for the beamwidth to be about 3^o at 10kHz, the primary frequencies can be calculated to give $2\theta_d \simeq 3^o$. Using the absorption data for seawater, it is found that the primary frequencies would need to be about 200kHz. The maximum primary source level which may be used without running into high-intensity effects would be

$$(SL)_1 = (SL)_2 \simeq 134 \text{ dB}$$

which would yield a difference-frequency source level of

$$(SL)_- \simeq 101 + 20 \log \frac{|V|}{\alpha_T r_o}$$

As can be seen from the Fig.2, for $\psi_y < 1$ the "correction" term is negative, hence the source level obtainable would be low.

As pointed out above, if $\psi_y \geq 1$, the difference-frequency beamwidth is largely controlled by the primary beamwidth. For a given difference frequency, $2\theta_d$ can be decreased by reducing the primary frequency. Further, if the primary beamwidth ($2\alpha_1$) is kept constant, ψ_y would be increased, providing higher values for the parameter $|V|\alpha_T r_o$ (see Fig.2). Also, as the primary source levels which may be used (without running into high intensity effects) will increase at the lower frequencies, higher difference-frequency source levels may be obtained.

This argument leads to the conclusion that it is best to choose the primary frequencies to be as low as possible. However, it must be remembered that the requirement that $2\alpha_1$ must be maintained constant (as the primary frequencies are reduced) results in an increase in the size of the transducer. Therefore, if the maximum size of the transducer is fixed, it would appear that an acceptable design could be obtained by choosing the mean primary frequency to be that which would provide the required primary beamwidth.

A further consideration is to allow for some beam-broadening (due to high-intensity effects) when the transmitting device is driven hard.

The IOS - University of Birmingham Proposal

In 1971 the University of Birmingham, Department of Electronic Engineering, were seeking a full scale application for a nonlinear sound source as a logical expression of confidence in the work done up to that time. At the same time IOS were becoming more and more interested in narrow beam echo-sounding. It was natural therefore, in view of the close liaison between the two establishments, to consider the possibilities of applying the idea of nonlinear sound generation to narrow beam bathymetry. First of all a paper study was carried out to compare various theoretical possibilities with the known performance of the IOS Precision Echo Sounder. The outcome of this study was a proposal for a system of the following characteristics:-

Transmitter

Primary frequency $(f_1 + \frac{\Delta f}{2})$	=	80kHz
Secondary frequency Δf	=	10kHz (with possibility of 3kHz for some applications)
Output power	=	1.5Kw acoustic per frequency of 6Kw acoustic peak envelope power
Transducer	=	40cm square
Beam width	=	3^{o}
Source level (at 1m)	=	+ 116dB rel µbm at 1 metre

In the construction phase of the transducer it was noted that it could be used more suitably at a mean frequency of 75kHz (i.e. at primary frequencies of 70 and 80kHz). The following results relate to the use of the parametric device at a centre frequency of 75kHz:-

For a salinity of 35‰, at a temperature of 10^{o}C, the absorption parameter α_T has a value of about 6.40×10^{-3} Np/m. For a difference-frequency of 10kHz,

$$\theta_d = \sqrt{2\alpha_T / k} = .0175 \text{ rads } (1.00 \text{ Deg.})$$

At 75kHz, $\lambda_0 = 2$cm, $\ell = 40$cm gives

$$\gamma_1 = \frac{\sqrt{2}}{\pi} (\lambda_0 / \ell) = .0225 \text{ rads } (1.29 \text{ Deg.})$$

Hence, $\psi_y = \gamma_1 / \theta_d = 1.29$

From Fig.1,

$$\text{Beamwidth} \simeq 2\gamma_1 \times 1.02 = 2.6 \text{ Deg.}$$

and from Fig.2,

$$20 \log \frac{|V|}{\alpha_{T^r}} = 1 \text{ dB}$$

At a frequency of 75kHz, the primary source levels can be made as high as 180.5 - 20 log 75 = 143 dB rel μbm (rms) without running into high intensity effects. [With a transducer area of 1600cm , this source level would be obtained with acoustic powers of about 3kW per frequency.] On this basis, the maximum effective source level which may be obtained at the difference-frequency would be

$$(SL)_{\text{max}} = -186.7 + 20 + 286 + 1$$

$$= 120 \text{ dB rel μbm (rms)}$$

It should be noted that the transmitted power mentioned above would correspond to intensities of 2 W/cm^2 per frequency, at the peak of the envelope of the composite wave producing intensities of about 8 W/cm^2, which would lead to severe cavitation problems. Also, one might expect some degradation of performance due to shock formation in the envelope peaks. To reduce the magnitude of both these problems, it was recommended that the transmitted power be reduced to about 1.6kW per frequency. On this basis, the effective source level at 10kHz would be expected to be about 114 dB rel μbm (rms).

To avoid cavitation at the surface of the transducer, it was decided that the transducer would be operated at a suitable depth.

Receiver

The IOS Precision Echo Sounder was thought to be suitable using either the standard transducer or the high frequency transducer in the flat low frequency part of its characteristic. In order to obtain large enough signal to noise ratios for automatic digitising the use of a long pulse and matched processor was to be included in the design. The division of labour assigned to IOS the task of producing the transducer and towing system, while Birmingham University would undertake the transmitter including the PPA. Accordingly NERC was approached with a request to give the University of Birmingham a contract for their part.

Technical Aspects of the Project

(a) The Transducer

It was clear at once that the transducer would present a real challenge in design, for the frequency relationships required a fairly high frequency (in ocean acoustic terms) transducer with a maximum Q of 8. The transducer also had to have an efficiency of at least 75% to keep the pulse power amplifier requirement within the reasonable limit of 10 Kwatts peak output, while still allowing for cable and tuning element losses. In addition it is difficult to make the active portion of the transducer more than about 40% of the aperture and this necessitates a power density of over 10 watts per square centimetre, which in turn requires the transducer to be operated at a depth of about 30 metres to avoid cavitation. The design is an extension of previous low frequency IOS designs using a pre-stressed sandwich of P2T-4 discs with brass tail masses and titanium conical radiating heads incorporating a mounting flange at the front face. Titanium is used to allow the radiating face direct contact with the water without fear of corrosion. Fig. 5 shows a cross section of the elements. The array is made up of a number of individual stacks, whose

dimensions were scaled from the earlier designs. This resulted in a large mumber of rather small assemblies, so to avoid scaling problems the titanium parts were machined in one piece from plate. However before this was done a protoype element was assembled and gave satisfactory results (11 watts/cm^2 at 90% efficiency and a Q of 6). Fig.6 shows the electrical admittance of a single element in air and Fig.7 is the equivalent circuit. After this a 3 x 3 array was constructed which again was satisfactory and ran at 11 watts/sq.cm. for an aggregate of 54 hours without failure. This array on the other hand had a rather higher Q of 10.5 when driven altogether, but driven individually the Q's were 7 or 8. This increase in Q was slightly worrying but not considered serious enough to hold up the full size array. It is the result of the dilution of the effectiveness of the baffle when all elements are driven and one would expect it to flatten out as the proportion of peripheral elements falls. The baffle which consists essentially of the interstitial metal is driven partly by the acoustic reaction of the water and partly via the small annulus of metal which forms the mounting flange. As the cone face is only 0.6 wavelengths in diameter both effects are finite, and the analysis is excessively complicated. The mutual radiation impedance between nearest neighbour elements is about 20% of the self radiation impedance and opposite in sign which undoubtedly contributes to the rise in Q. The effect of compliant coupling to the baffle is much harder to guess the effect of, but both effects can be mitigated in future designs by adopting the largest possible radiating cone. For the large array a chance had to be taken that the effect would flatten off fairly quickly. We return to this point later. The full scale array consisted of 729 elements on a 27 x 27 matrix 43 cms square. It turned out that the individual element Q minimised at 75 KHz so the tail mass was trimmed accordingly. In the machining operation only one station was lost though tool breakthrough when cutting annulus to within 0.5mm of a 12mm thick plate, and this was blanked off with epoxy resin. Conventionally a piezoelectric transducer is constructed by reversing the polarity of adjacent discs and bringing out electrodes from each joint thereby driving the discs electrically in parallel but mechanically in series. This design however had 4 discs which would have meant five electrodes and ten epoxy joints, leading to a very compliant and low impedance stack. To avoid this the discs were aligned in pairs and two reversed pairs formed a stack. Also the return path was taken through the titanium plate, using the tail mass and pre-stressing bolt to contact the back of each stack. As well as reducing the number of glued joints to 6, and increasing the array impedance by a factor of 4, this approach reduced the number of connecting wires to manageable proportions. A flat glass reinforced nylon cover was provided for the back of the transducer plate, and the hydrostatic pressure supported by a set of Tufnol pillars, one for each transducer, spigoted and glued in the gaps between the transducers. The pillars were drilled horizontally to take busbor wires supplying drive to the live electrodes via flexible connector wires. Electrical connection was made to the supply cable via glands led through the front of the transducer plate. The glueing, wiring and prestressing of the elements were straightforward enough but required skill and care. Figs. 10 and 11 show the transducer construction.

The completed array when tested in water had a resonant frequency of 73.7KHz, and impedance of 5.3Ω and a Q of 13.8, Fig.8 shows admittance diagrams of array + 200m of cable with and without shunt choke. It was impossible to get a meaningful Q in air for the whole array, but the elements were tested individually on pre-stressing when they had Q values ranging from 35 to 140 with a mean of at least 70. The efficiency calculated from these Q values

is at least 80% so the design was met in this respect. The loaded Q for the whole array is rather more than double the single element value, indicating the extent to which the effects discussed earlier do go. In the full size array only 13% of elements are edge elements compared with about 90% for the 9 element array. The effect of high Q is two-fold. Firstly it reduces the array admittance at the edge of the operating frequency band, so that with a voltage limitation on the drive the power at the band edges is much reduced. Secondly it makes the compensation for reactive admittance over the operating band more difficult. The present project however does not require operation over the whole band but merely at the two extreme edges. For this reason it is possible to adjust the PPA output transformer to match the reduced load admittance, and to provide slightly more complicated reactive compensation to make the admittances real and equal at both frequencies of interest. The actual band spread about the two operating frequencies (due to the limited pulse lengths) is an order of magnitude smaller than the separation, so pulse envelope distortion is not a problem. The purpose of the first trials was primarily to test the transducer and PPA and to check the actual secondary source levels obtained. A secondary objective was to assess the interface requirements with the Precision Echo Sounder. The problem of transducer stabilisation was shelved until the acoustic side of the project had been proved. For this reason the transducer was mounted on a simple welded steel framework and fitted with an unfaired cable, it being accepted that the trials would be conducted hove to.

The Pulse Power Amplifier

The University of Birmingham were given a contract by NERC to produce an amplifier capable of providing 10 KW electrical into a 10 ohm load in 5 mS pulses each second. The amplifier had to be proof against both short and open-circuit loads, and to present no special difficulties in servicing and repair. To avoid adding unnecessarily to the hazards at sea it was decided at the outset to use transistors throughout if possible.

The outcome of comparative cost studies for various transistor types and groupings, was a system of eight modules. Each module is a self-contained amplifier with an isolated high impedance output, and the eight outputs are paralleled so that the output currents are summed in the load. Since each module is short circuit proof the amplifier can be run with any number of modules missing at correspondingly reduced power. The modules each have 30 general purpose power transistors working in class B push-pull, into a 90 mm ferroxcube pot-core transformer. The main architecture of the amplifier is very successful but there are a lot of details both electrical and mechanical within the modules which need attention, before it can be described as a finished product.

The Receiver

For the first sea trials it was desirable to have as much versatility as possible. For instance an acoustic calibration of the primary source level requires a high frequency receiving channel, also it was desirable to be able to measure the secondary echoes as received on both the Precision Echo Sounder and the high frequency transducer. For this reason a separate receiver unit was constructed at IOS, with facilities for generating the required transmitted pulses and receiving via any desired channel. In addition there were transducer voltage and current monitors. The other trials feature was a long transmitted pulse with a swept difference frequency, varying linearly with time. The frequency band was much the same,

but the pulse lasted 28 mS instead of the short pulse 2.8 mS, so that its energy content was 10 times as great. By feeding the pulse through a dispersive delay line the energy in the pulse can be compressed thereby increasing the signal to noise ratio. The pulse in use had a signal/noise gain of 10dB. Cook and Bernfield /5/ deal with the subject quite exhaustively in connection with radar but the theory applies without change to sonar. The net effect is a 10dB increase in effective source level which may well be an essential pre-requisite to automatic digitisation of depth measurements. In view of the energy drain from the PPA power supply during those long pulses, the power supply was fitted with a matching set of lead acid accumulators. In fact the power supply voltage of the PPA is 36v so three accumulators were required which were called upon to provide current pulses in excess of 100 amperes.

The First Sea Trials

The transducer, PPA and receiver were taken to sea from October 5 to October 11 1974 in RRS Discovery. After the usual difficulties with new equipment the trials proper commenced with admittance tests on the transducer. Particular care was taken to ensure that the transducer face was well wetted, as a very small quantity of air could cause distortion of the admittance diagram and ruin the Q. Furthermore the application of full power could easily destroy the elements near the air bubbles. Efficient wetting was confirmed by monitoring the admittance diagram to ensure that it remained stable with time and coincided with the one obtained in the test tank. This test period was also used to adjust the parallel choke to provide the best conpensation of cable and clamped array capacity. Fig.8 shows the uncompensated and compensated admittance diagram in seawater at 30 metres depth.

Power handling tests showed that the transducer had not approached its power handling limit with the PPA at full output. The PPA had delivered 5 Kw into its dummy load with little distortion, but into the transducer the maximum power obtainable at 75 KHz was 3.5 KW. The power measurements during the twin frequency pulses were as follows: See Fig. 12.

-6dB drive level	Peak Voltage	410v p.p.	) giving	V	= 250v p.p.
	Valley "	90v p.p.	)	V	= 160v p.p.
-3dB " "	Peak Volts	780v p.p.	) giving	V	= 455v p.p.
	Valley "	130v p.p.	)	V	= 325v p.p.
OdB " "	Peak Volts	840v p.p.	) - envelopes distorted so		
	Valley "	160v p.p.	) no individual voltages		
			) available.		

Because the amplifier was showing signs of instability at the OdB drive level, the -3dB level was used for the tests, this actually giving a better geometric mean power than the OdB drive. The power into the water was calculated by using the measured admittance at each frequency and then applying the efficiency to the geometric mean power, as follows at the -3dB drive level:-

80 KHz - $Y = (.0525 - jx.0615)$ mho $\quad \frac{(455)^2}{8} \times .0525 = 1358W$

70 KHz - $Y = (.066 + jx.059)$ mho $\quad \frac{(325)^2}{8} \times .066 = 871W$

Geometric mean power = 1087W

Estimated acoustic power (= 78%) = 848 watts per frequency.

Expected secondary source level at -3dB drive = +109.5dB re 1 mBar rms
and at - 6dB drive = +98dB re 1 mBar rms.

In calibrating the non-linear sound source the bottom was used as a target. The bottom was flat and fairly smooth mud and gravel under 150 metres of water. The ship was hove to with a certain amount of pitching. Reception was carried out on both the high frequency transducer and the 10 KHz Precision Echo Sounder, and calibration using the known sensitivity of the latter and the free-field sensitivity of the former computed from the admittance circles using the reciprocity relation. In both cases the echo, after calibrated gain, was displayed on an oscilloscope with delayed trigger from the transmitted pulse. In both cases the echo showed large fluctuations in amplitude and these were highly correlated with delay, being very much smaller for the later arrivals. The total travel time was 370 m sec minimum and very small pulses could be seen as late as 385 mS. Because both transducers had a receiving beam-width of about 20^{o} the receiving beam geometry would have to change at about 30^{o} per second to make any great difference to sensitivity between transmission and reception, and the variations would not be highly correlated with delay. For these reasons it was concluded with a fair degree of confidence that the fluctuations were due to geometrical back-scattering effects as discussed in a previous section. The half-angle of the cone in which the transmitting transducer was swinging would be given by arc cos 370/385 = 16^{o}, a result which fits in quite well with the back-scattering diagram, fig.2, and with the sort of swing one would expect from the ship motion with a light and slightly un-balanced transducer fish. For these reasons the maximum echo amplitude was taken for calibration purposes as this represented normal incidence and a true bottom loss figure. With this the figures are as follows:-

A) Calibration using high frequency transducer;

Round trip 213 metres - spreading loss 46.6dB
Bottom loss 12.0dB
Attenuating negligible
Total losses 58.6dB

Largest echo = 3.2v p.p. at output of amplifier
= 10 mV on transducer o/p
= + 80dB re 1 mV p.p.

Transducer sensitivity = + 20.5dB re 1 mV/mBar.

Free-field pressure = + 59.5dB re 1 mBar p.p.
= + 50.4dB re 1 mBar r.m.s.

Source level (1m) = 50.4 + 58.6 = + 109dB re 1 mBar r.m.s.

compared with the expected level of + 109.5dB

B) Calibration using Precision Echo Sounder;

Round trip = 750 metres spreading loss = 57.5dB
Bottom loss = 12 dB
Total = 69.5dB

Echo (at 6v p.p.) = + 66.5dB re 1 mV r.m.s.

Gain = 38.4dB

Transducer o/p = 66.5 - 38.4 = + 28.1dB re 1 mV r.m.s.

= + 88.1dB re 1 mV r.m.s.

Sensitivity = + 48.1dB re 1 mV/mBar

F.f pressure = 88.1 - 48.1 = + 40dB re 1 mBar r.m.s.

Source level (1m) = + 40 + 69.5 = 109.5dB re 1 mBar r.m.s.

This agreement is indicative of the accuracy of the respective transducer calibrations but for an absolute calibration it depends on the accuracy of the bottom loss figure. Unfortunately it was not realised until too late that this measurement had been omitted. An opportunity must be taken to put this right as soon as possible, but in the meantime the calibration must have limits of error put on it. It is almost certain that the bottom loss falls within the range 9 - 15dB as virtually all reported measurements lie in the range 6 - 18dB and the bottom was neither bare rock nor soft mud. The important conclusion is that the non-linear transmission system is capable of giving source levels comparable with the precision echo sounder, namely + 116dB, provided the full power capability of the transducer can be used, and with the 10dB processing gain of the stretched pulse a sufficient signal excess for successful digitising in many situations could be obtained. Fig.13 is a record obtained in shallow water with the non-linear source, and clearly throws the pulse to pulse variability caused by fish pitch.

Work Remaining to be Done

Before the system can be routinely taken to sea by non-specialist personnel certain items of work remain to be done. The largest and most obvious job is to develop and construct a pitch stable towed vehicle to house the array, and since the acoustics are now demonstrated, work on this has started.

As already mentioned the Pulse Power Amplifier needs rebuilding with partial re-design of the modules and this also has been started.

A further job concerns the compensating network for the load. Since the transducer is capacitive the full potential of the power amplifier can only be reached if the array is shunted by a choke which just cancels the effect of the excess capacity. On the other hand we are trying to drive the array at two frequencies simultaneously and require compensation at two frequencies. This can be done with a two pole network as follows:- From Fig.8 which is the admittance diagram of the transducer in water plus the cable we read off the admittance values at the respective operating frequencies. Let these be $G_1 + jB_1$ and $G_2 + jB_2$. We need a single network which has the admittances $-jB_1$ and $-jB_2$ at f_1 and f_2 respectively. If f_1 is less than f_2 and $G_1 = G_2$ (which is approximately true, since f_1 and f_2 are symmetrically placed about f_o), then we need a network whose admittance is purely inductive and falls with increasing frequency in the range f_1 to f_2. We can then choose the elements of the network so that exact match is obtained at f_1 and f_2. Such a network is a series tuned circuit above its resonant frequency, the admittance of which is given by:-

$$Y = \frac{j\omega C}{1 - \omega^2 LC} = -B_1 \text{ at } \omega = \omega_1$$

$$= -B_2 \text{ at } \omega = \omega_2$$

Thus $\omega_1 , c = \omega_1^2 B_1 \; LC - B_1$

and $\omega_2 = \omega_2^2 B_2 \; LC - B_2$

from which L and C can be determined in terms of B_1. B_2, ω_1 and ω_2 to give

$$L = \frac{\omega_2 B_1 - \omega_1 B_2}{B_1 B_2 (\omega_2^2 - \omega_1^2)}$$

and C can be found by re-substitution.

Using these formulae and choosing f_1 and f_2 such that $f_2 - f_1 = 10.2$ KHz (the required operating difference frequency) and $G_1 = G_2$ we get:-

f_1 = 69.7 KHz f_2 = 79.9 KHz B_1 = j .163 mho B_2= jx .005 mho

L = 1.622 mH C = 3,242 pF

This network is resonant at 69.4 KHz. which is very close to f_1 at 69.7 KHz, the reason being that B_2 is so near to zero. The result is that if the compensation for B_1 is to be at all stable the network elements L and C must be stable to better than .05% under all operating conditions. Fig.9 shows the effect this compensating network has on the admittance circle. It is intended to include both this and the plain choke compensation so that the most suitable can be switched in.

Finally a certain amount of work remains to be done on the interfacing to the Precision Echo Sounder, but the details of the way in which the results will be displayed and used, depend on the results of operational experience, so that the integration of the non-linear source into the Echo Sounder system is the third and last development phase of the work.

References

[1] Camp.1 Underwater Acoustics Wiley Interscience 1970

[2] Tolstoy I. and Clay C.S. Ocean Acoustics McGraw-Hill 1966

[3] Patterson R.B. J.A.S.A. Vol 36 No.6 pp. 1150-54 1964

[4] Westervelt P.J. J.A.S.A. Vol 29 p. 199 1957

[5] Cook F.C. and Bernfeld M. Radar Signals Academic Press 1967

Figures

APPENDIX

Introductory treatment of the theory of Parametric Transmitters

Small-signal analysis

The exact differential equations of acoustic wave propogation in a homogeneous fluid are nonlinear. This observation was made by scientists of 18th and 19th century. Lord Rayleigh[1] and Lamb[2] comment on the earlier attempts at solving the exact equations. Blackstock[3] has provided a more up-to-date historical survey of the topic.

Ideas on the possible exploitation of the nonlinear effects in acoustic wave propagation are much more recent.

Westervelt[4] applied some ideas of Lighthill's on the generation of sound by turbulence to the scattering of sound by sound. His basic result was an inhomogeneous wave equation representing the scattered wave parameters in terms of the primary field. Paraphrasing his result, the scattered field may be ascribed to a volumetric source distribution, the strength of which (per unit volume) is given by

$$q = (\beta/\rho_o^2 c_o^4) \frac{\delta}{\delta t} p_i^2 \qquad (1)$$

where p_i is the excess (acoustic) pressure at the source point, ρ_o and c_o are, respectively equilibrium density of and the sound velocity in the medium.

β is a parameter of nonlinearity, and is related to the pressure-density relationship in the medium. If the isentropic pressure-density relationship is expanded in the form of a Taylor's series around the equilibrium values, one may write

$$p_T = p_o + \left(\frac{dp}{d\rho}\right)_o (\rho_T - \rho_o) + \tfrac{1}{2} \frac{d^2 p}{d\rho^2} (\rho_T - \rho_o)^2 \qquad (2)$$

where the subscript T has been used to indicate the total values of the parameters, while subscript o is used for the equilibrium values. (It is found that for water, all the higher-order terms may be neglected without loss). If this equation is now written in the form

$$p_T - p_o = A \left[(\rho_T - \rho_o)/\rho_o \right] + (B/2) \left[(\rho_T - \rho_o)/\rho_o \right]^2 \qquad (3)$$

where A and B are related to the differential coefficients given in Equation 2,

$$\beta = 1 + B/2A \qquad (4)$$

For water, at normal temperatures, B/A has a value of the order of 5 which gives $\beta \simeq 3.5$. (This value of β has been found to give good agreement between estimated and measured values of scattered pressure in nonlinear devices.)

For mathematical formulation of the scattered component of acoustic wave, it is easier to work in terms of the Fourier transform of the source function, as defined in Equation 1. If $Q(\omega)$ is the Fourier transform of $q(t)$ at a source-point $(x', y', z'$, say) then, the scattered pressure at a field point (x, y, z) will have a Fourier transform

$$P_s(\omega) = (j\omega\rho_o/4\pi) \iiint \frac{Q(\omega).\exp[-(\alpha + jk)s]}{s}.\, dx'dy'dz' \qquad (5)$$

where s is the magnitude of the vector joining the field-point to the source-point, and the volume integral includes all the sources. It must be noted that Equation 5 is correct (and exact) if the scattered waves are not involved in any further nonlinear interactions. This, then, is a statement of the single-scattering (or quasi-linear) approach to the analysis of the nonlinear effects. In practice, it means that the value of p_i at a source-point is estimated on the basis of the primary (radiated) waves alone, this expression for p_i is used in Equation 1 to evaluate the source-function, the Fourier transform of which (in turn) is used in Equation 5 to evaluate the scattered field.

[It must be stressed that this, the single-scattering approach, has severe limitations in the analysis of nonlinear phenomena in may cases. But, in estimating the characteristics of parametric transmitters, this approach has been found to provide sufficiently accurate results.]

A simple application of this technique to the parametric transmitters is due to Westervelt[5]. He considered the primary field to consist of two superposed plane waves (of frequencies ω_1 and ω_2) which were confined within a very narrow column. The primary pressure field can then be represented in the form

$$p_i = p_1 + p_2 \qquad (6)$$

where

$$p_1 = p_1 e^{-\alpha_1 x'} \cos(\omega_1 t - k_1 x')$$

and

$$p_2 = p_1 e^{-\alpha_2 x'} \cos(\omega_2 t - k_2 x') \qquad (7)$$

it being understood that p_i is zero outside the column.

As a result of the nonlinear interaction between these two waves, new components (at interaction frequencies) are generated. If ω_1 and ω_2 are of the same order of magnitude, the difference-frequency component may be at a much lower frequency than either of the primary waves, and hence subject to a much lower rate of absorption. This is the component which is utilized in parametric transmitting devices.

The source-function at the difference-frequency can be calculated from Equations 1 and 6. The only term in the expression for p which can give rise to the difference-frequency component is $2p_1 p_2$. A simple manipulation of Equations 7 and 1 yields

$$q_- = -\left(k_-\beta P_1 P_2/\rho_0^2\ c_0^3 \right) .\quad \exp\left[-(\alpha_1 + \alpha_2)x' \right] .\ \sin(\omega_- t - k_- x') \qquad (8)$$

where the subscript (-) is used to indicate the values of the various parameters pertaining to the difference-frequency component. Representing this in complex notation, one obtains

$$Q_- = \left(jk_-\beta P_1 P_2/\rho_0^2\ c_0^3 \right) \exp\left[-(\alpha_1 + \alpha_2 + jk_-)x' \right] \qquad (9)$$

Substitution in Equation 5 yields

$$P_- = \left(k_-^2\ \beta P_1 P_2/4\pi\rho_0\ c_0^2 \right) . \iiint \frac{1}{s} \cdot \exp\left[-(\alpha_1+\alpha_2+jk_-)x' - (\alpha_- + jk_-)s \right] . \\ dx'\ dy'\ dz' \qquad (10)$$

For long-range applications, a far-field approximation can be made for s , thus simplifying the integral. If the field point is well beyond the effective inter-action distance of the primary waves (i.e., the distance for which $(\alpha_1 + \alpha_2)\ x' >> 1$) then we may substitute in the integrand

$1/R$ for $1/s$

and $k_-(R - x' \cos\theta)$ for $k_- s$.

Further, if the cross-sectional dimensions of the column are small compared with the wavelength at the difference-frequency, integration with respect to y' and z' introduces the cross-sectional area, S, as a factor, and Equation 10 becomes

$$P_- \simeq -(k_-^2\ \beta P_1 P_2 S/4\pi\rho_0\ c_0^2\ R)\ \exp.\left[-(\alpha_- + jk_-)R \right] \\ \int_{x'=0}^{\infty} \exp\left\{ -\left[\alpha_T + jk_-\ (1 - \cos\theta) \right] x' \right\} . dx; \qquad (11)$$

where $\alpha_T = \alpha_1 + \alpha_2 - \alpha_-$ (12)

The integral in Equation 11 yields

$$1 / \left[\alpha_T + jk_-\ (1 - \cos\theta) \right]$$

which may be used to re-write Equation 11 in the form

$$P_-(R,\theta) \simeq P_W(R,o) .\ D_R(\theta) \qquad (13)$$

where

$$P_W(R,o) = -\frac{k_-^2 \beta P_1 P_2 S}{4\pi \rho_o c_o^2 \alpha_T R} \cdot \exp[-(\alpha_- + jk_-)R], \quad (14)$$

and

$$D_R(\theta) = 1 / [1 + j(k_-/\alpha_T)(1 - \cos\theta)] \quad (15)$$

Thus, the difference-frequency waves may be represented in the form of a spherically-spreading wave, with a complex directivity function given by $D_R(\theta)$.

For water, the ratio k_-/α_T can be made large. Then, the magnitude of $D_R(\theta)$ can have significant values only for small values of θ. For $|\theta| \ll 1$, $1 - \cos\theta \simeq \theta^2/2$, and Equation 15 gives

$$|D_R(\theta)| \simeq [1 + (k_- \theta^2/2\alpha_T)^2]^{-\frac{1}{2}} \quad (16)$$

Hence, if we represent the 3dB beamwidth (associated with $D_R(\theta)$ by $2\theta_d$,

$$\theta_d = \sqrt{2\alpha_T/k_-} \quad (17)$$

α_T is controlled mainly by the absorption at the primary frequencies, while k_- is the wave-number at the difference-frequency. Hence, the beamwidth ($2\theta_d$) obtainable at a particular difference-frequency may be controlled by choosing the primary frequencies appropriately.

[It should be noted that although this analysis pertains to an idealized model, the parameter θ_d has been found to be very useful in the normalization of the characteristics of parametric transmitters.]

Equation 14 can be used to estimate the effective source-level at the difference-frequency. This can be represented by P'_-, where

$$P'_- = |R\, P_W(R,O).\exp(\alpha_- R)| \simeq \frac{k_-^2 \beta P_1 P_2 S}{4\pi \rho_o c_o^2 \alpha_T} \quad (18)$$

For future reference, this result will now be put in a different format. The two primary frequencies are assumed to be of the same order of magnitude and the wavelength at the centre-frequency is taken to be λ_o. If S represents the active area of a transducer, the near-field distance at the primary frequencies would be

$$R_o = S/\lambda_o,$$
$$\text{i.e.} = k_o S/2\pi \quad (19)$$

The primary source levels (given by P_1' and P_2' respectively) can be related to P_1 P_2 and R_0 :-

$$P_1' \simeq P_1 R_0 \quad \text{and} \quad P_2' \simeq P_2 R_0 \tag{20}$$

Using these expressions in Equation 18, a simple manipulation yields

$$P_-' \simeq \frac{k_- \beta P_1' P_2'}{2\rho c_0^2 \alpha_T r_0} \tag{21}$$

where $$r_0 = (k_0/k_-) R_0 \tag{22}$$

k_0/k_- is sometimes referred to as the "downshift ratio", being the ratio of the mean primary frequencies to the difference frequency. Similarly, r_0 is referred to as the "collimation distance" in more general treatment of the parametric transmitters.

Another format for the difference-frequency source level can be obtained in terms of the acoustic powers transmitted at the two primary-frequencies, W_1 and W_2. As

$W_{1,2} = P_{1,2}^2 / 2\rho_0 c_0$, Equation 18 gives

$$P_-' \simeq \frac{k_-^2 \beta}{2\pi c_0 \alpha_T} \sqrt{(W_1 W_2)} \tag{23}$$

For water, using $c = 1500$ m/s and $\beta = 3.5$, this expression yields

$$\text{R.M.S. Source-level} \simeq -27 + 40 \log F_- + 10 \log (W_1 W_2) - 20 \log \alpha_T \quad \text{dB rel } \mu\text{bm} \tag{24}$$

where F_- is the difference-frequency in kHz, W_1 and W_2 are in watts and α_T in Np/m.

In practical applications of parametric transmitters, one would envisage transmitting the two primary waves from the same transducer assembly. For the purposes of this report only a square transducer assembly (producing a quasi-conical beam) will be considered.

An acoustic wave radiated from such a transducer (of area S) can be assumed to be confined within a column of cross-sectional area (approximately) S up to the near-field distance R_0 , and then spreading spherically, with a directivity pattern which depends upon the size of the transducer in terms of the wave-length at the transmitted frequency. If such a transducer is used in a parametric transmitter, if $\alpha_T R_0 \gg 1$, the effective interaction region is confined within the near-field. Then, the analysis presented above for the case of collimated primary waves is applicable. On the other hand, if the bulk of the interaction takes place in the far-field of the transducer, then a different model must be used. The following treatment is discussed in

detail in reference 6. A simplified form is included here for completeness.

The primary waves may now be represented in the following (complex) form:-

$$P_{1,2} = (p'_{1,2}/r)\ D_0(\gamma, \phi).\ \exp\left[-(\alpha_{1,2} + jk_{1,2})r\right] \qquad (25)$$

where $D_0(\gamma, \phi)$ represents a two dimensional directivity function.

From Equation 1, the difference-frequency source-function can be obtained. Using the far-field approximations, and the expression for the elemental volume

$$dv = r^2 \cos\gamma \ d\gamma \ d\phi \ dr$$

in the scattering integral, one obtains (after integration with respect to r between the limits o and ∞)

$$P_- = (R, \theta, \eta) \simeq \left(k_-^2\ p'_1\ p'_2\ \beta/4\pi\ \rho_0\ c_0^2 \alpha_T R\right) \exp\left[-(\alpha_- + jk_-)R\right] \qquad (26)$$

$$\int_{-\pi/2}^{\pi/2}\int \frac{D_0^2(\gamma, \phi)\ \cos\gamma\ d\gamma\ d\phi}{1 + j(k_-/\alpha_T)(1-u)}$$

where $u = \cos\gamma\ \cos\theta \cos(\phi - \eta) + \sin\gamma\ \sin\theta$ (27)

If all the angles may be assumed to be small (relying on the weighting by the square of the primary directivity pattern to reduce errors) the expression (1 - u) may be replaced by

$$\tfrac{1}{2}\left[(\gamma - \theta)^2 + (\phi - \eta)^2\right]$$

and the integral becomes, approximately,

$$(\text{Int.}) \simeq \iint \frac{D_0^2(\gamma, \phi)\ d\gamma\ d\phi}{1 + j\left[\left(\frac{\theta - \gamma}{\theta_d}\right)^2 + \left(\frac{\eta - \phi}{\theta_d}\right)^2\right]}$$

Also, a simple manipulation of Equation 26 (with the aid of Equations 19 and 20) reduces it to the form

$$P_- = (R, \theta, \eta) = P_W(R, o) \cdot (S/\lambda_0^2) \cdot (\text{Int.}) \qquad (29)$$

where P_W (R,o) is the expression given in Equation 14.

At this stage, it is worthwhile to consider the form of the directivity function $D_o(\cdot)$.

For a square transducer of sides $\ell = L\lambda_o$, where L >> 1

$$D_o(\gamma, \phi) \simeq \frac{\sin(\pi L\gamma)}{\pi L\gamma} \cdot \frac{\sin(\pi L\phi)}{\pi L\phi} \tag{30}$$

If the 3dB beamwidth in $\gamma = 0$ (or in $\phi = 0$)plane is $2\gamma_1$

$$\gamma_1 \simeq \sqrt{2}/\pi L \tag{31}$$

It is proposed to represent the integrand in Equation 28 in terms of normalized angles,

$$\gamma' = \gamma/\theta_d \quad \text{and} \quad \phi' = \phi/\theta_d \tag{32}$$

clearly,

$$\begin{aligned} \pi L\gamma &= \sqrt{2} \cdot (\theta_d/\gamma_1)\, \gamma' \\ \pi L\phi &= \sqrt{2} \cdot (\theta_d/\gamma_1)\, \phi' \end{aligned} \tag{33}$$

Thus, using a new parameter

$$\psi_y = \gamma_1/\theta_d \tag{34}$$

$$D_o(\gamma, \phi) = \frac{\sin\left(\sqrt{2}\,\gamma'/\psi_y\right)}{\sqrt{2}\,\gamma'/\psi_y} \cdot \frac{\sin\left(\sqrt{2}\,\phi'/\psi_y\right)}{\sqrt{2}\,\phi'/\psi_y}$$

$$\equiv D_\psi(\gamma', \phi'), \quad \text{say} \tag{35}$$

(It is worth pointing out that ψ_y is the ratio of the beamwidth of the primary waves to $2\theta_d$.)

By inspection of Equation 28, one obtains

$$(S/\lambda_o^2).\ (\text{Int.}) \;=\; (S\theta_d^2/\lambda_o^2) \iint \frac{D_\psi^2\,(\gamma',\,\phi').\ d\gamma'\,d\phi'}{1 + j\,[(\theta' - \gamma') + (\eta' - \phi')]}$$

$$V_\psi\ (\theta',\ \eta'),\ \text{say} \qquad (36)$$

Here, $\theta' = \theta/\theta_d$ and $\eta' = \eta/\theta_d$. From Equations 29 and 36, the difference-frequency pressure field can be represented in the form

$$p_-\ (R,\ \theta,\ \eta) \;=\; P_W\ (R,o).\quad V_\psi\ (\theta',\ \eta'). \qquad (37)$$

$V_\psi\ (\theta',\ \eta')$ was evaluated numerically, for various values of the parameter ψ_y, over a range of values of θ' and η'. From these computed results, both the magnitude of V_ψ (o, o) and the 3dB beamwidth of the difference-frequency field (normalized with respect to $2\theta_d$) were obtained for various values of ψ_y. These results are given in Reference 6. Here, it is proposed to present these results in a different form, to facilitate a comparison with the results presented by Mellen and Moffet[7], after a slightly different treatment of the scattering integral discussed above.

Mellen and Moffett use as their basic parameter $\alpha_T r_o$ where α_T is the total absorption given in Equation 12, and r_o is the "collimation distance" given in Equation 22. Their result for the difference-frequency sound pressure along the axis of the acoustic beam may be written in the form (valid for $R >> r_o$)

$$p_-\ (R,o,o) \;=\; P_W(R,o).\ \Big\{\ 1 - \exp\,(-\alpha_T r_o)\ + j\,\alpha_T r_o\ \big[E_1\ (\alpha_T r_o) - E_1\ (\alpha_T R)\big]\Big\}\ , \qquad (38)$$

where $E_1\ (x) \;=\; \int_x^\infty (1/t)\,\exp\,(-t).\ dt.$

This result has the advantage that a "propagation curve" can be provided for the difference-frequency waves, albeit for ranges greater than r_o.

It can be shown quite simply that the parameters $\alpha_T r_o$ and ψ_y are related to one another:-

$$\alpha_T r_o \;=\; \alpha_T R_o \cdot k_o/k_-$$

$$\text{i.e.,} \;=\; (\alpha_T \rho^2/2\pi)\ (k_o^2/k_-)$$

$$\psi_y = \gamma_1 / \theta_d$$

$$\text{i.e.,} = 2\sqrt{2/k_o \rho}\ \theta_d$$

$$\text{i.e.,} = 2\left[\alpha_T \rho^2 k_o^2 / k_-\right]^{-\frac{1}{2}}$$

Hence, $$\alpha_T r_o = 2/\pi \psi_y^2 \qquad (39)$$

Thus the results of references 6 and 7 can be compared directly.

The 3dB beamwidth of the difference-frequency waves (normalized with respect to $2\theta_d$ and with respect to the beamwidth of the primary waves) is shown plotted in Fig.14 against ψ_y. Also shown are the corresponding values of $\alpha_T r_o$.

Effective source level at the difference-frequency can be estimated from Equations 37 and 21 (the latter provides, effectively, the contribution of $P_W(R,o)$ to the source level). Then, the difference-frequency source level (peak) is

$$\hat{(SL)}_- = 20 \log P'_-\ ,$$

where

$$P'_- = \frac{k_- \beta P'_1 P'_2}{2\rho_o c_o^2} \cdot \frac{1}{\alpha_T r_o} \left| V(o,o) \right| \qquad (40)$$

For water, this yeilds for r.m.s. source-level,

(41)

$$(SL) = -186.7 + 20 \log F_- + (SL)_1 + (SL)_2 + 20 \log \frac{|V|}{\alpha_T r_o} \quad \text{dB rel } \mu\text{bm}$$

where $(SL)_1$ and $(SL)_2$ are the primary source levels (r.m.s.) in dB rel μbm. The parameter $20 \log \frac{|V|}{\alpha_T r_o}$ is shown plotted in Fig.15 against ψ_y. These results agree quite well with those obtained using Mellen and Moffett's model. Also they have been checked against all available experimental data, and have been found very reliable, so long as the intensities transmitted were such that the use of the single-scattering approach (on which the present analysis was based) could be justified.

High-intensity effects

If a single sinewave is transmitted with sufficient intensity, as it propagates the wave becomes progressively distorted, and eventually a shock-front is formed. Absorption at the steep shock-front is much greater than the absorption of the low-level signals, and the amplitude of the wave becomes attenuated very rapidly.

These high-intensity effects are very much smaller in a spreading wave, as the spreading loss decreases the local intensity, thereby reducing the rate of distortion.

A thorough treatment of these higher-order effects are outside the scope of the present report. Let it suffice that if the intensities transmitted are kept at such levels that the wave is not permitted to form shocks within the nearfield of a transducer, then the single-scattering approach provides acceptable agreement with experimental results.

If the shock-formation occurs well within the nearfield of the transducer, the extra-attenuation of the primary waves results in the reduction of the effective source level at the difference-frequency (as compared with the value estimated from Equation 41) accompanied with the broadening of the beam. In some, close-range applications of parametric transmitters (for example, for shallow penetration into sediments in shallow waters) such deleterious effects may not be too disadvantageous. However, for a long-range, narrow-beam echo-sounder application, these effects should be kept to a minimum.

The shock-formation distance for a sinusoidal plane wave, in the absence of absorption, is given by

$$x_{CR} = \rho_0 c_0^2 / \beta P_0 k_0 \quad ,$$

which, for water, reduces to

$$x_{CR} = 10^8 \lambda_0 / P_0 \qquad (42)$$

Here P_0 is in Pascals (N/m^2) and is the initial pressure amplitude. If this is compared with the near-field R_0, it is required that R_0/x_{CR} is of the order of or less than unity. That is,

$$P_0 R_0 / 10^8 \lambda_0 \leq 1 \quad .$$

$$\text{i.e.,} \quad P_0' / 10^8 \lambda_0 \leq 1 \qquad (43)$$

For example, for $\lambda_0 = 0.02$m (i.e., at 75kHz)

$$P_0' \quad 2 \times 10^6 \quad (N/m^2)m$$

which corresponds to a peak source level of 146 dB rel μbm.

[Mellen and Moffett's "Saturation parameter" is based in this concept. If $R_0/x_{CR} = X$, the condition discussed here corresponds to $X \leq 1$. Remembering that for water $\lambda_0 \simeq 1.5/F_0$ m. where F_0 is the mean primary frequency in kHz, Equation 43 gives

$$X = P_0' F_0 / 1.5 \times 10^8,$$

and $X = 1$ corresponds to a peak primary source level $(SL)_0$ given by

$$(SL)_0 + 20 \log F_0 = 183.5 \text{ dB rel}\mu\text{bm}.$$

The expression on the left-hand side of this equation is the "scaled source level" used by Mellen and Moffett.]

REFERENCES

1. LORD RAYLEIGH "The Theory of Sound". Dover Publications.

2. LAMB, H. "The Dynamical Theory of Sound". Dover Publications.

3. BLACKSTOCK, D.T. "History of Nonlinear Acoustics and a Survey of Burgers' and Related Equations" in the Proc. of the symposium on Nonlinear Acoustics held in Austin, Texas (1969).

4. WESTERVELT, P.J. J.A.S.A. 29, 199 (1957).

5. WESTERVELT, P.J. J.A.S.A. 35, 535 (1963).

6. BERKTAY, H.O. and LEAHY, D.J. J.A.S.A. 55, 539 (1974).

7. MELLEN, R.H. and MOFFETT, M.B. "A Model for Parametric Sonar Radiator Design". N.U.S.C. Technical Memorandum No. PA 41-229-71 (1971).

CAPTIONS FOR FIGURES

Fig.13 Normalized beamwidth of the difference frequency waves.

Fig.14 Plot of the parameter $20 \log \frac{|V|}{\alpha_T r_o}$

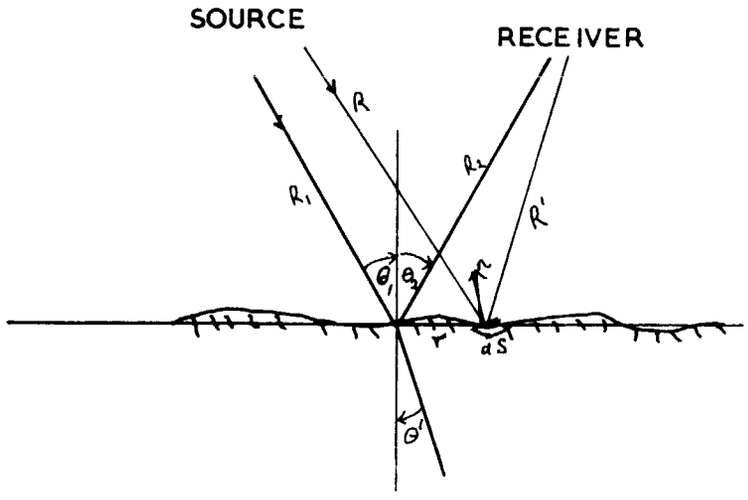

FIG 1 SCATTERING AT A ROUGH SURFACE

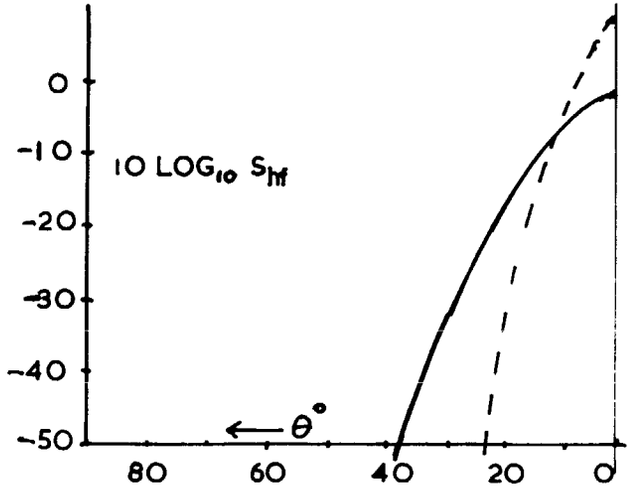

FIG 2 BACKSCATTERING FUNCTION

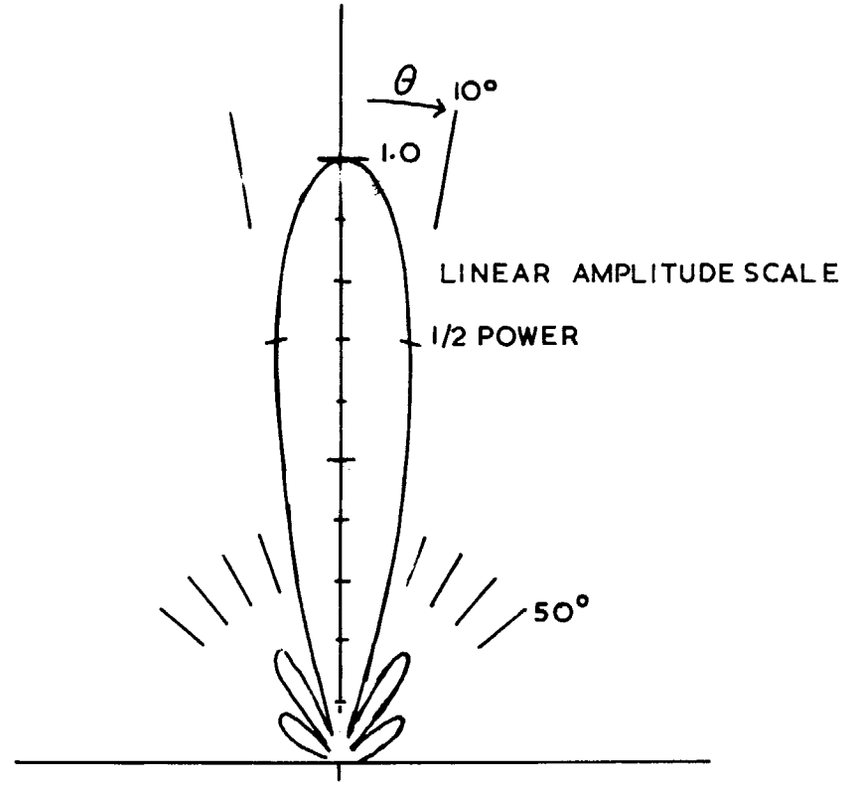

FIG 3 BEAM PATTERN OF 3λ LINE ARRAY

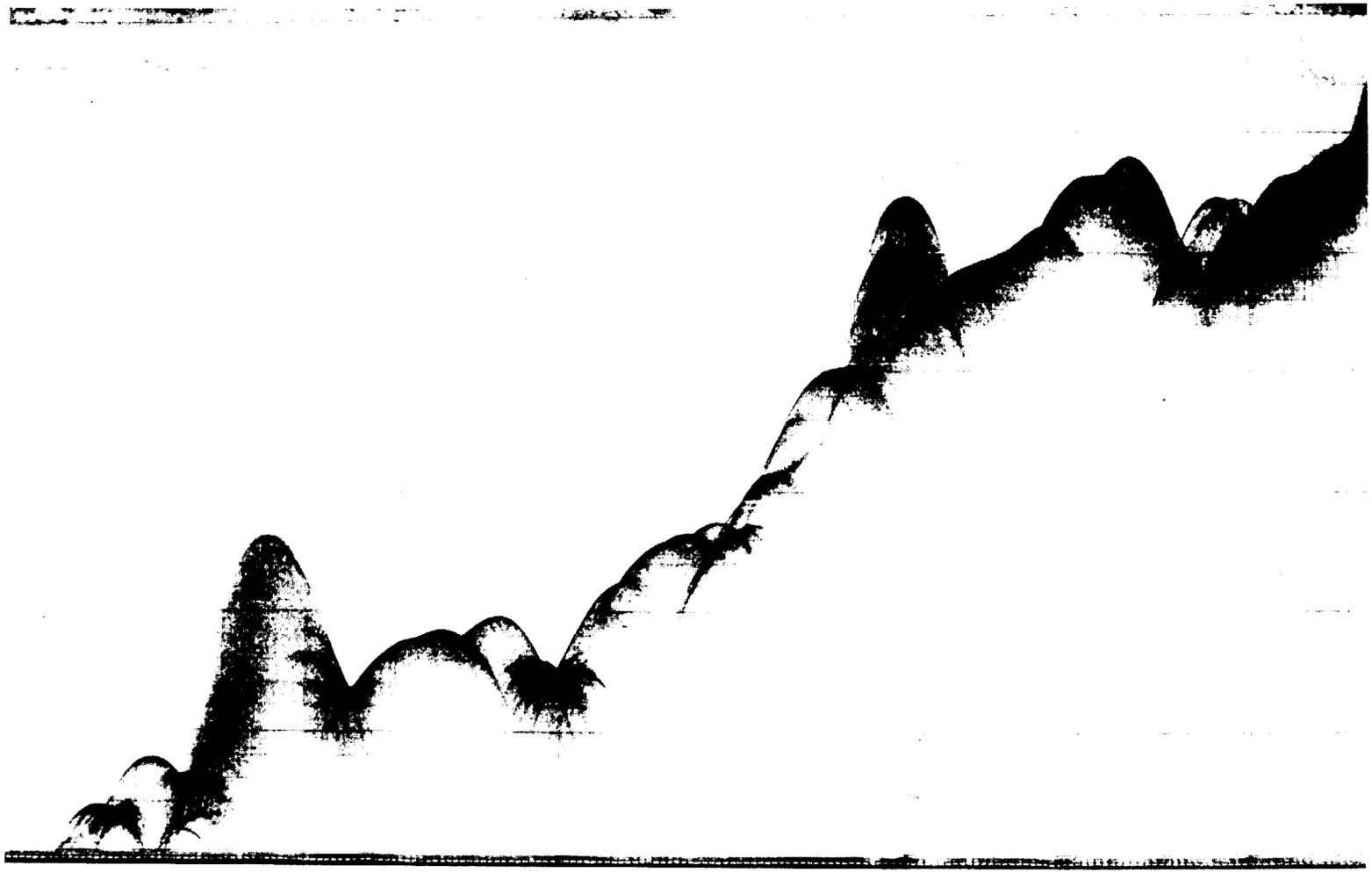

FIG 4 WIDE BEAM ECHO-SOUNDER RECORD

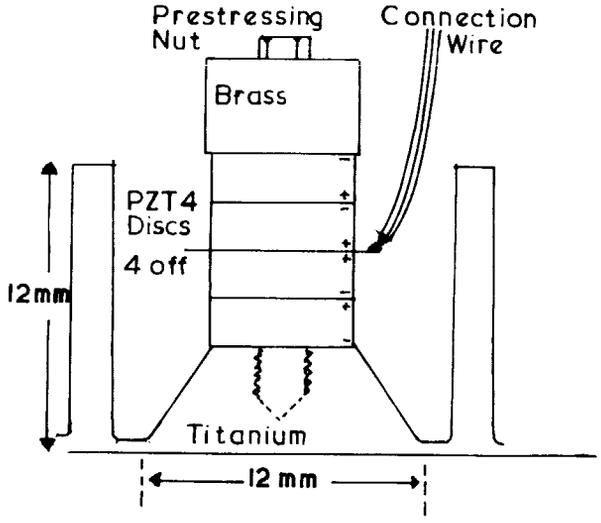

FIG 5 CROSS SECTION OF 75 KHz TRANSDUCER ELEMENT

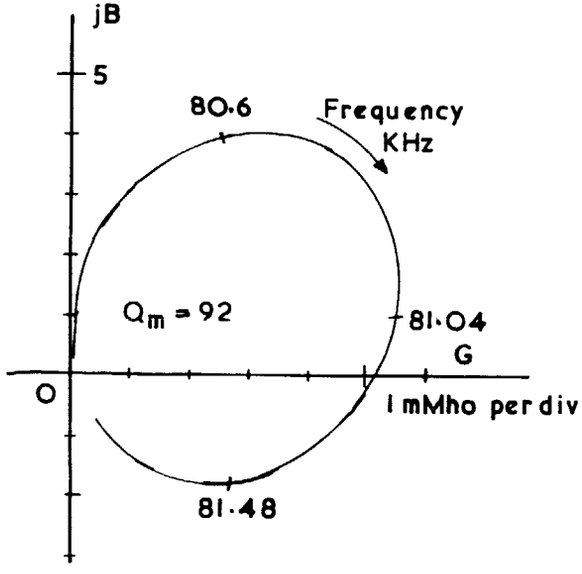

FIG 6 ADMITTANCE DIAGRAM OF A SINGLE ELEMENT IN AIR

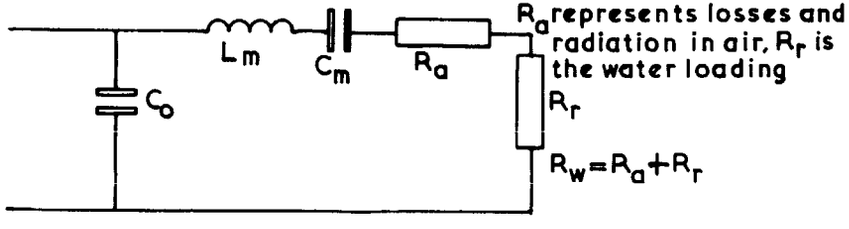

FIG 7 APPROXIMATE EQUIVALENT CIRCUIT OF AN ELEMENT

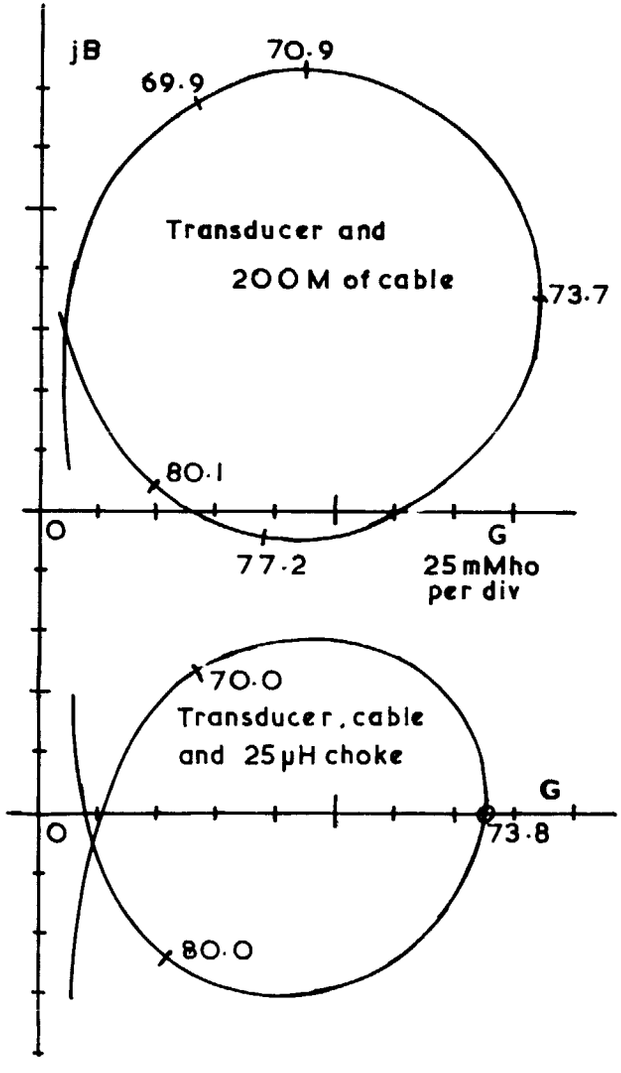

FIG 8 ADMITTANCE DIAGRAMS OF COMPLETE ARRAY WITH AND WITHOUT COMPENSATING CHOKE

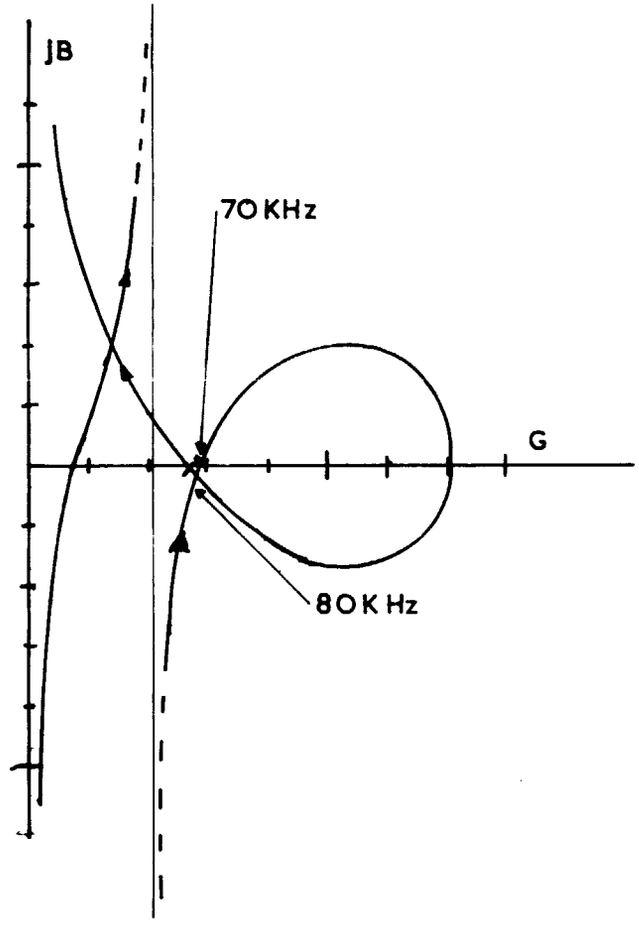

FIG 9 SHOWING THE EFFECT OF SERIES L-C COMPENSATION

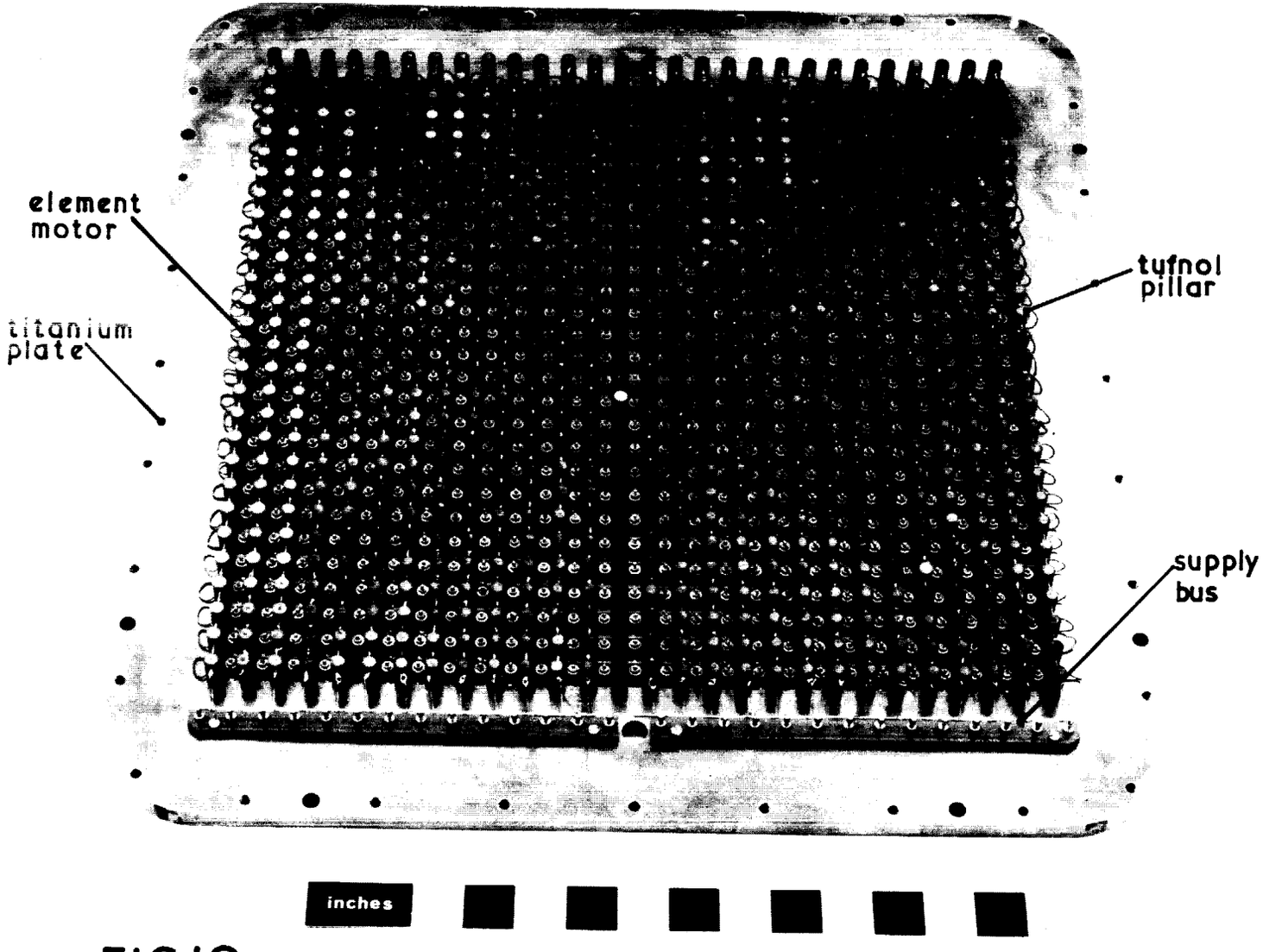

FIG 10 ASSEMBLED TRANSDUCER REAR VIEW

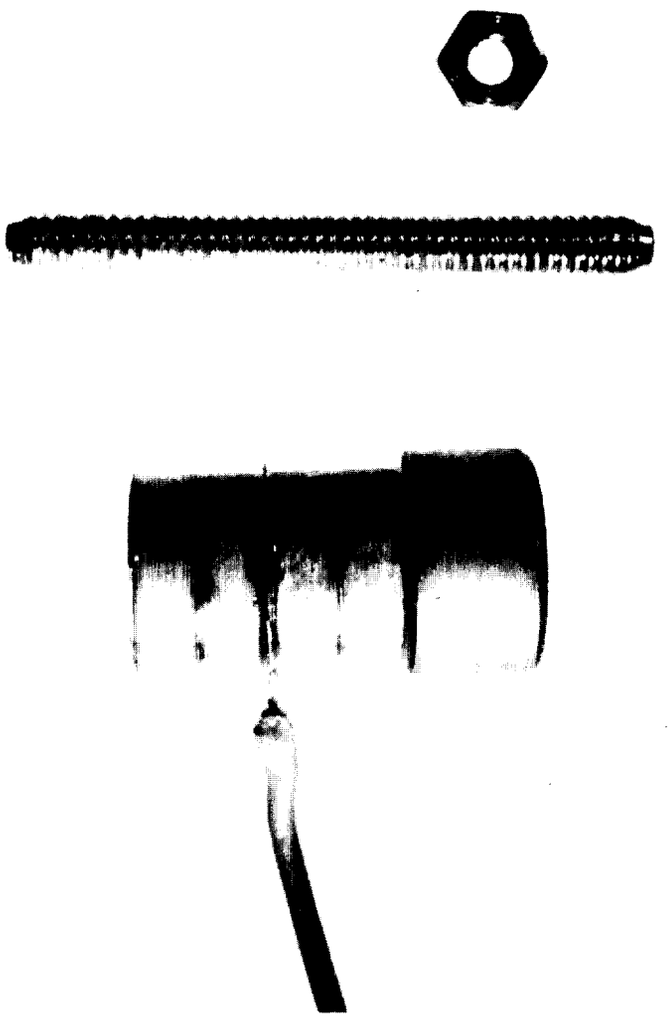

FIG 11 MOTOR AND PRESTRESSING BOLT READY FOR ASSEMBLY TO PLATE

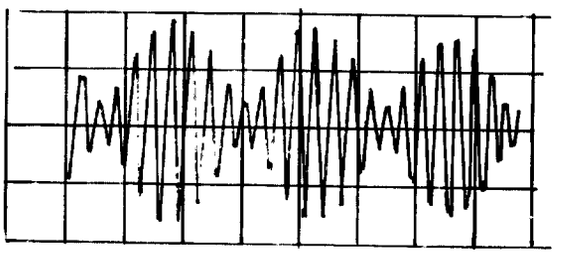

−6 dB DRIVE 100V/div

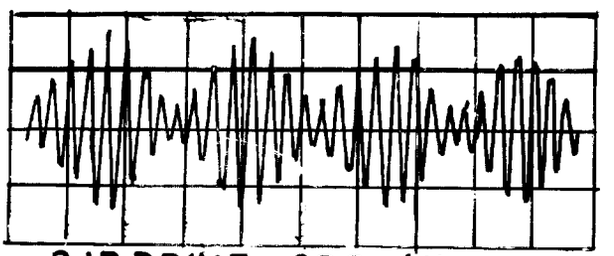

−3dB DRIVE 200 v/div

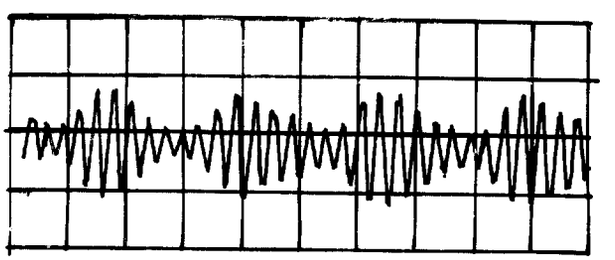

OdB DRIVE 400 v/div

FIG 12 TRANSDUCER TERMINAL VOLTAGE WAVEFORMS HORIZONTAL SCALE 50μSEC/DIV

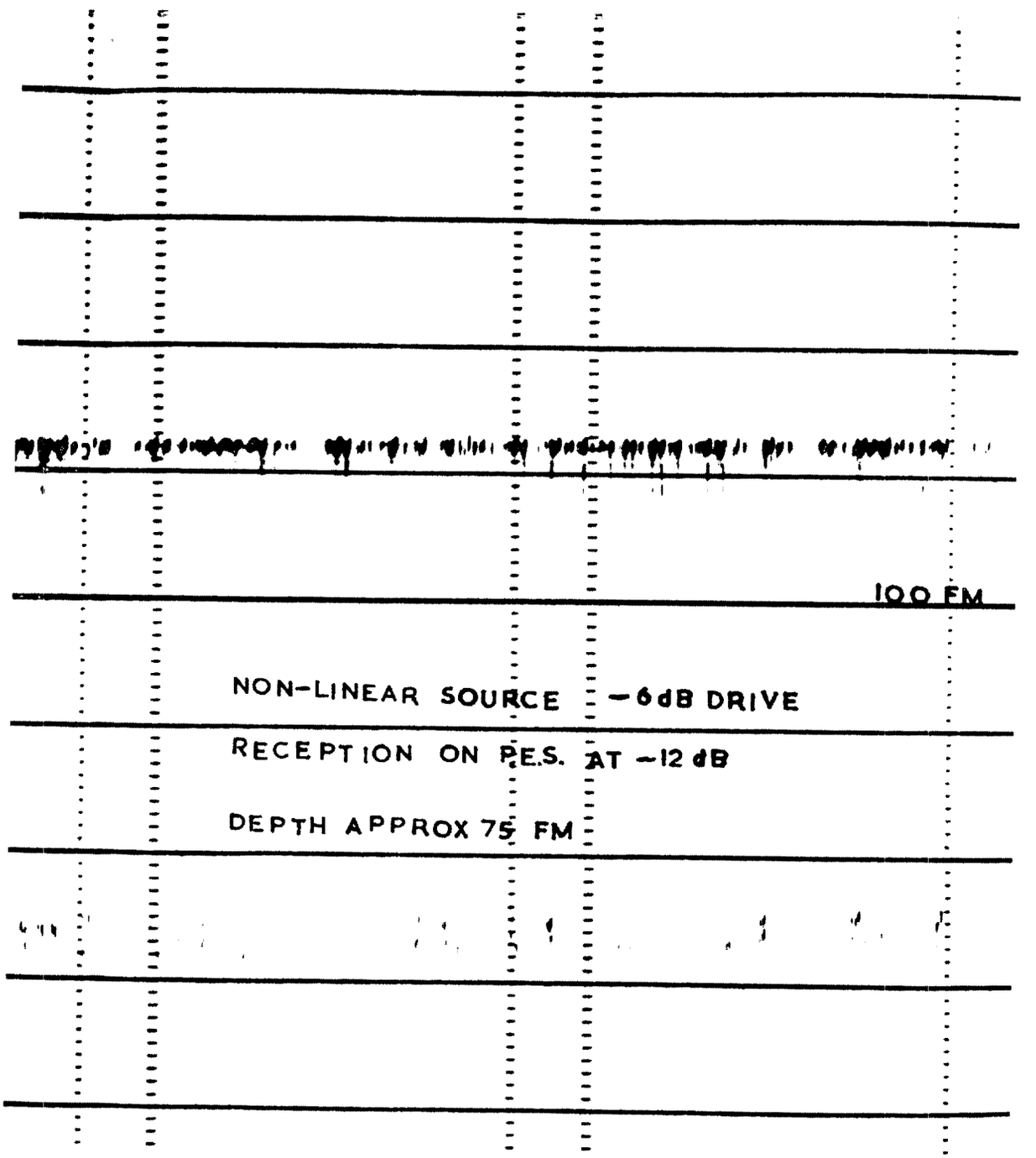
100 FM
NON-LINEAR SOURCE -6dB DRIVE
RECEPTION ON P.E.S. AT -12 dB
DEPTH APPROX 75 FM

FIG 13

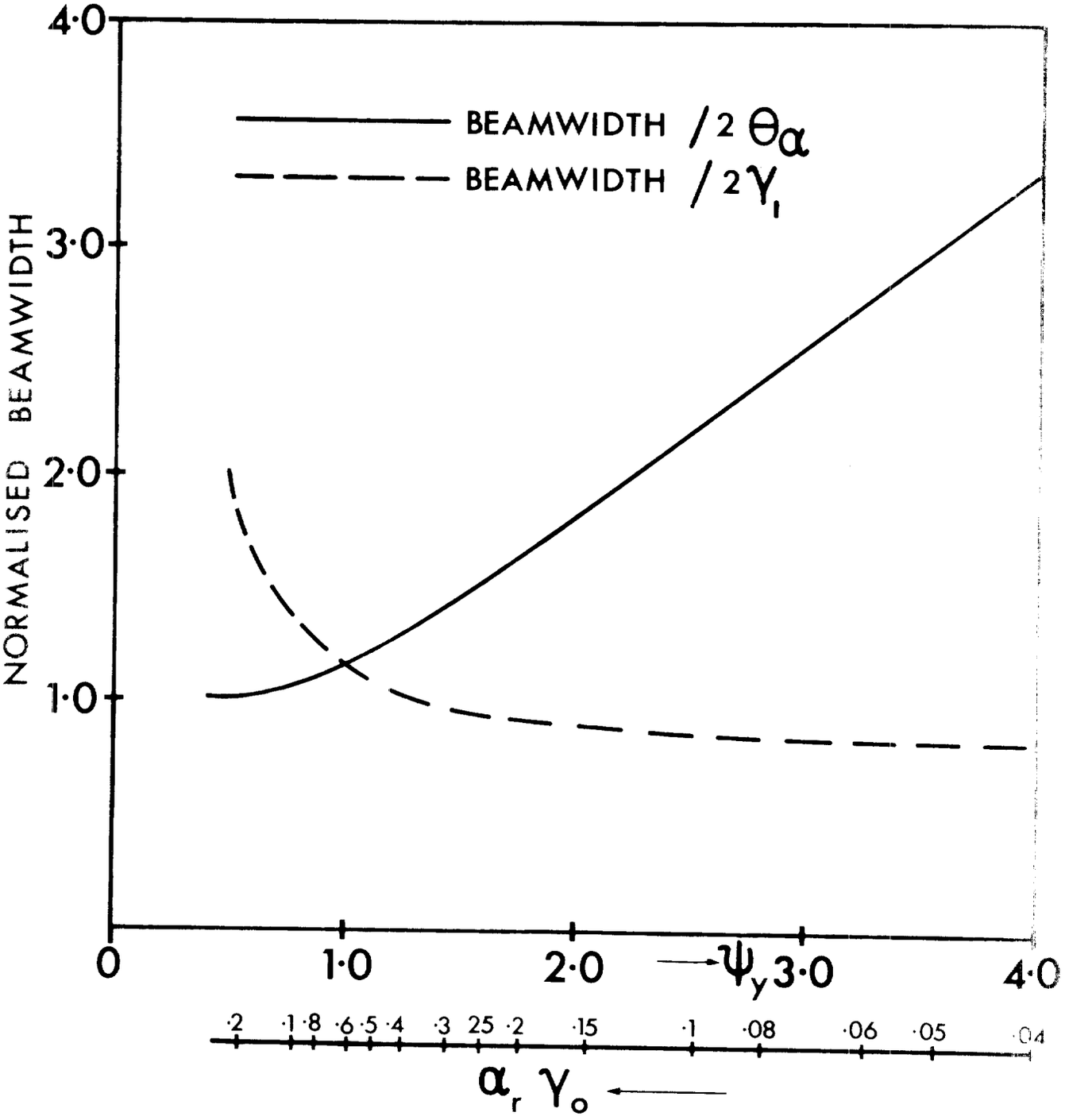

FIG. 14. Normalised beamwidth of the difference frequency waves

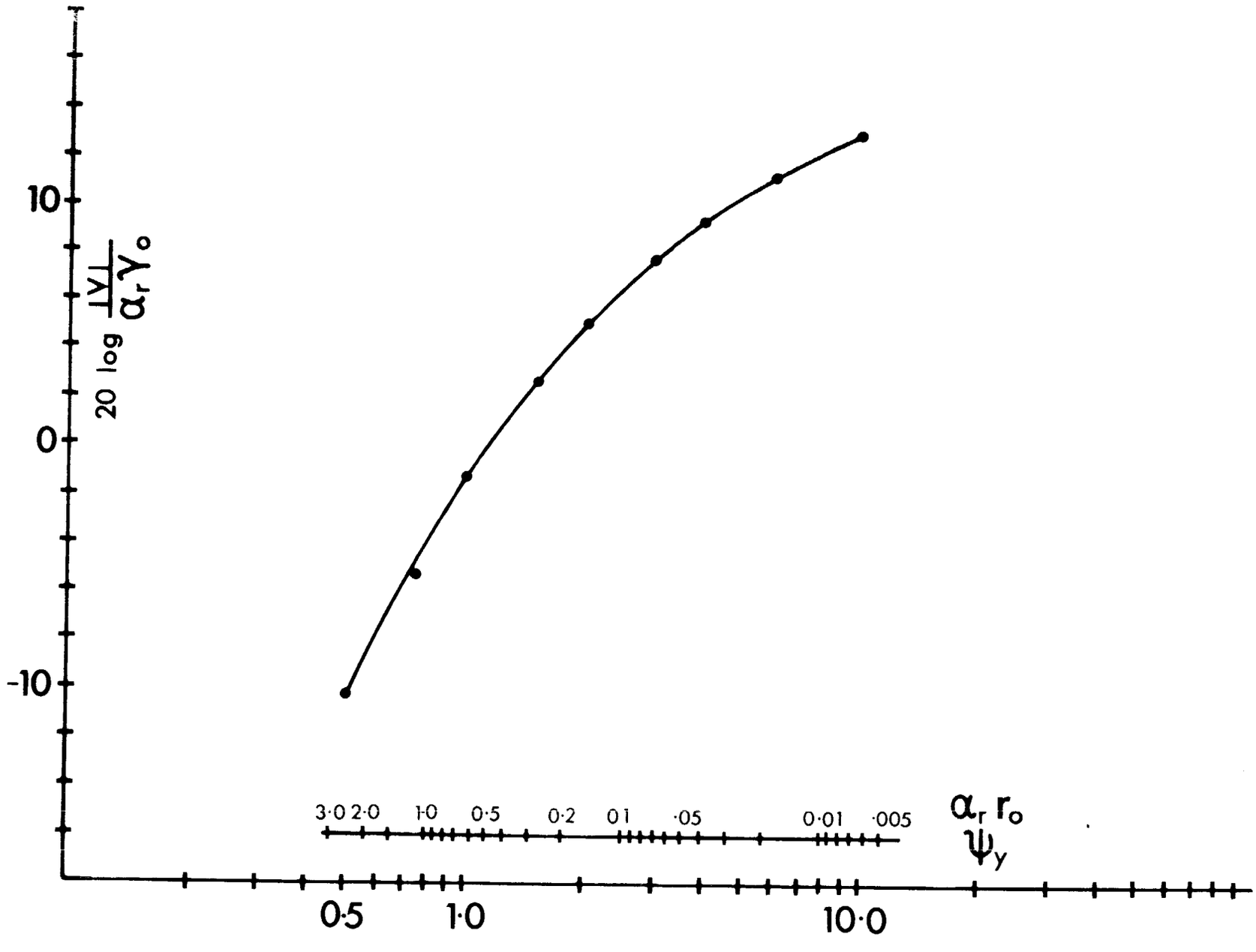

FIG. 15 Plot of the parameter $20 \log_{10} \frac{|V|}{\alpha_r r_o}$

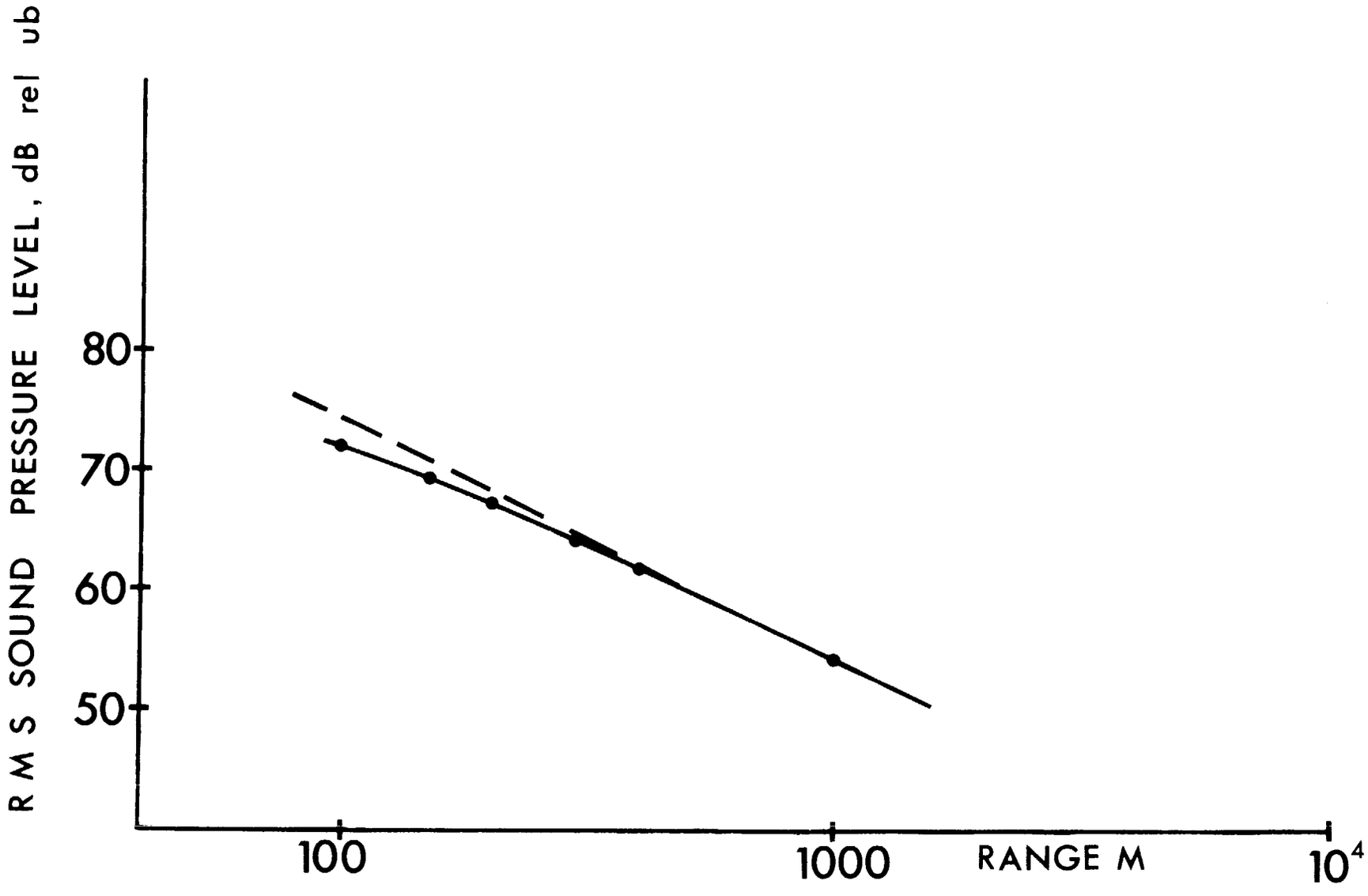

FIG. 16 Estimated propagation curve at 10 KHz